

AMERICAN UNIVERSITY OF BEIRUT

INVESTIGATING NAPROXEN REMOVAL FROM
PHARMACEUTICAL FACTORY EFFLUENTS USING NOVEL
MIL-88-A/PS/UVA AND MIL-88-A/PS/SOLAR SYSTEMS.

by

SARAH GHANEM GHAZALI

A thesis
submitted in partial fulfillment of the requirements
for the degree of Master of Science
to the Department of Chemistry
of the Faculty of Arts and Sciences
at the American University of Beirut

Beirut, Lebanon
January 2022

AMERICAN UNIVERSITY OF BEIRUT

INVESTIGATING NAPROXEN REMOVAL FROM
PHARMACEUTICAL FACTORY EFFLUENTS USING NOVEL
MIL-88-A/PS/UVA AND MIL-88-A/PS/SOLAR SYSTEMS.

by
SARAH GHANEM GHAZALI

Approved by:

Dr. Antoine Ghauch, Professor
Department of Chemistry

Advisor



Dr. Digambara Patra, Professor
Department of Chemistry

Digambara Patra

Member of Committee

Dr. Kamal Bouhadir, Professor
Department of Chemistry

Member of Committee



Date of thesis defense: January 25, 2022

ACKNOWLEDGMENTS

This thesis becomes a reality with the kind of support and help of many individuals. I would like to extend my sincere thanks to all of them.

Foremost, I would like to express my sincere gratitude to my thesis supervisor Dr. Antoine Ghauch for the continuous support of my thesis study and research, for his patience, motivation, and immense knowledge. His advice was invaluable during the research and writing of this thesis.

Besides my advisor, I would like to thank my thesis committee: Dr. Kamal Bouhadir and Dr. Digambara Patra for their encouragement and insightful comments.

We are also grateful to Dr. Mario El Kazzi, group leader in the electrochemical Energy Storage Section at the Paul Scherrer Institute, for performing and interpreting the XPS study, as well as Dr. Maxim Yilkov, who assisted with the EPR analysis and simulations at ETH, Switzerland.

A superb job also necessitates the collaboration of a group of people. This is accomplished by the American University of Beirut (AUB), which provided us with the opportunity to get superior education as well as work with the most advanced machines to complete our experimental work. Special thanks go to the academic and non-academic staff of the Chemistry department, as well as the staff of the KAS CRSL, for their efforts in keeping the research work flowing.

My thanks and appreciation also go to my lab mates and graduate colleagues: Abbas, Zahraa, Suha, Rime, Weam and Fatat who have willingly helped me out with their abilities and for maintaining a pleasant work environment.

Finally, a special thanks to my family. No words can express how grateful I am for all the sacrifices that you have made on my behalf. Your prayers for me have kept me going so far. Without their endless love, support, and drive, I would not have been able to achieve my goals.

ABSTRACT OF THE THESIS OF

Sarah Ghanem Ghazali

for

Master of Science

Major: Chemistry

Title: Investigating Naproxen Removal from Pharmaceutical Factory Effluents using Novel MIL-88-A/PS/UVA and MIL-88-A/PS/Solar Systems.

Safe disposal of the pharmaceutical industry wastewater is a major challenge for developing countries. Conventional wastewater treatment technologies relying on biological treatment were proven to be inefficient in the removal of such compounds. The toxic and stable nature of the compounds led to negative effects on the performance of municipal wastewater treatment plants necessitating the need to adopt at-source treatment solutions. Advanced oxidation processes (AOPs) are the at-source technologies adopted for the elimination of pharmaceuticals and other persistent organic pollutants. AOPs can be applied using several oxidants out of which persulfate (PS) is showing promising results. PS can undergo, chemical, UV and/or thermal activation. PS generates sulfate radicals upon its activation which has properties not found in hydroxyl radicals. Recently, heterogeneous activation of PS has gained attention in the research community for the possibility to reclaim the activator or pack it into a filtration media. Metal-Organic Frameworks (MOFs), are a highly porous material with excellent catalytic properties that are a great candidate to be tested as an activating agent in PS-based AOPs. MIL-88-A, an iron-based MOF, characterized by its stability, reusability, and environmentally friendly synthesis process will be used in our research as a model MOF. The aim will be to eliminate Naproxen (NAP), a non-steroidal anti-inflammatory drug (NSAID) and a widely used pharmaceutical, from simulated wastewater. The research will focus on the use of solar energy versus UVA/UVB radiation for the activation of MIL-88-A which will activate PS in order to eliminate NAP. MIL-88-A was synthesized and characterized to pursue this research. Preliminary experiments have been conducted to check MIL-88-A/PS activation. The system was optimized and tested for its recyclability, reproducibility and matrix variations. In UVA/MIL-88-A/PS system the % degradation of NAP ($[NAP]_0 = 50$ ppm) was 87.2% occurred in period of two hours and 40 minutes, and total degradation of NAP ($[NAP]_0 = 50$ ppm) occurred in 10-15 minutes in a system of Solar/MIL-88-A/PS.

Keywords: MOF, AOPs, Naproxen, MIL-88-A, persulfate

TABLE OF CONTENTS

ACKNOWLEDGMENTS	1
ABSTRACT	2
TABLE OF CONTENTS	3
ILLUSTRATIONS	5
TABLES	8
ABBREVIATIONS	9
INTRODUCTION	10
1.1 PPCPs as emergent contaminants.....	10
1.2 Persulfate based AOPs.....	11
1.3 Activation techniques	12
1.4 Metal organic frameworks (MOFs): properties and characteristics	12
1.5 MOFs in adsorption and catalysis	13
1.6 Naproxen as a target/model molecule.....	15
1.7 The choice of MIL-88-A in the study.....	16
1.8 Objective.....	17
MATERIALS AND METHODS	18
2.1. Chemicals.....	18
2.2. Synthesis of MIL-88-A	19
2.3. Characterization of MIL-88-A.....	19

2.4.	Experimental conditions and procedure	21
2.5.	Reaction setup.....	22
2.6.	Chemical analysis	23
RESULTS AND DISCUSSION		26
3.1.	Characterization of MIL-88-A.....	26
3.1.1.	XRD pattern of MIL-88-A	26
3.1.2.	SEM images of MIL-88-A	27
3.1.3.	BET analysis of MIL-88-A	28
3.1.4.	TGA and FTIR analysis of MIL-88-A	29
3.1.5.	XPS analysis of MIL-88-A.....	32
3.1.6.	TOF SIMS technique.....	34
3.2.	MIL-88-A/PS system controls	36
3.3.	UVA/MIL-88-A/PS system	38
3.3.1.	Effect of NAP dosage.....	41
3.3.2.	Recyclability.....	42
3.4.	Solar/MIL-88-A/PS system	45
3.5.	Matrix effect	49
3.5.1.	Case of chlorides	49
3.5.2.	Case of carbonates	51
3.5.3.	Case of phosphate.....	54
3.5.4.	pH effect	57
3.5.5.	EPR measurements	60
3.5.6.	Degradation mechanism	65
CONCLUSION		71
REFERENCES		72

ILLUSTRATIONS

Figure

1. Chemical structure of Naproxen.....	15
2. Illustration of MIL-88-A structure.....	16
3. Experimental Setup of a) MIL-88-A/PS/UVA/NAP and b) MIL-88-A/PS/Solar/NAP systems.....	23
4. Emission spectrum of the UVA mosquito lamps used in the experiment	23
5. (a) Calibration curve of NAP. The error bars are calculated at 95% confidence level. Absorbance = A (mean) $\pm tsn$, where t is the student value ($t = 2.447$ for 6 degrees of freedom at 95% confidence level) and s the standard deviation of 7 replicates. (b) The LINEST output calculated through Excel provided the slope, y intercept, the regression coefficient and all statistical data including standard deviations on variables.	25
6. XRD diffraction pattern of MIL-88-A.....	26
7. SEM of crystals of MIL-88-A at different magnifications	27
8. BET adsorption/desorption isotherms of MIL-88-A [69].....	28
9. TGA analysis of MIL-88-A [69]	30
10. TGA-FTIR analysis of the synthesized MIL-88-A [69].....	31
11. XPS analysis of pristine MIL-88-A and used MIL-88-A in UVA-free and UVA-irradiated systems after the oxidation reaction. (a) XPS survey spectra, (b) Fe $2p_{3/2-1/2}$ spectra, (c) O1s spectra and (d) C1s spectra. XPS spectra of all samples are almost overlap	33
12. TOF-SIMS positive spectra of (a) MIL-88-A as prepared, (b) NAP powder, (c) MIL-88-A after use in the presence of NAP and (d) MIL-88-A after use in the presence of NAP and PS. The spectra are normalized to the Bi $_3^+$ received dose and have the same y axis scale. Areas of the spectra are multiplied by 5 or by 2 for visual purposes.	35
13. Elimination of NAP in a combined MIL-88-A/PS system and in the presence of MIL-88-A only and PS only under UVA light. Experimental conditions: $[NAP]_0 = 50$ ppm, $[PS]_0 = 2$ mM, $[MIL-88-A]_0 = 25$ mg L $^{-1}$. Error bars are calculated as tsn , where absent bars fall within the symbols.	37
14. The % degradation of NAP irradiated with UVA lamps as function of time (min) in three reactions under different conditions: PS only, MIL-88-A only, and MIL-88-A with PS. Reactors were irradiated by the UVA lamps placed on the side. Experimental	

conditions: $[NAP]_0 = 50$ ppm, $[PS]_0 = 2$ mM, $[MIL-88-A]_0 = 25$ mg L ⁻¹ . Error bars are calculated as <i>tsn</i> , where absent bars fall within the symbols.....	39
15. Chromatogram of NAP extracted at 228 nm showing the by-products formed at 6.30, 8.06 and 9.79 min, respectively under UVA irradiation in UVA/MIL-88-A/PS system.	40
16. Effect of NAP concentration on NAP degradation. Experimental conditions: $[PS]_0 = 2$ mM, $[MIL-88-A]_0 = 25$ mg L ⁻¹ . Error bars are calculated as <i>tsn</i> , where absent bars fall within the symbols.	41
17. Recyclability experiments of MIL-88-A in the UVA reactors. $[NAP]_0 = 50$ mg L ⁻¹ . $[PS]_0 = 2$ mM, $[MIL-88-A]_0 = 25$ mg L ⁻¹ . Error bars are calculated as <i>tsn</i> , where absent bars fall within the symbols.	43
18. SEM images of recycled MIL-88-A	44
19. XRD pattern of newly synthesized and recycled MIL-88-A	45
20. The % degradation of NAP irradiated with solar energy as function of time (min) under different conditions: PS only, MIL-88-A only, and MIL-88-A with PS. Reactors were put under sunlight in a rotisserie shaker. Experimental conditions: $[NAP]_0 = 50$ mg L ⁻¹ , $[PS]_0 = 2$ mM, $[MIL-88-A]_0 = 25$ mg L ⁻¹ . Error bars are calculated as <i>tsn</i> , where absent bars fall within the symbols.	46
21. Graphs showing the degradation of the by-products in Solar/MIL-88-A/PS system controls in the presence and/or absence of MIL-88-A and PS. Experimental conditions: $[NAP]_0 = 50$ mg L ⁻¹ , $[PS]_0 = 2$ mM, $[MIL-88-A]_0 = 25$ mg L ⁻¹	47
2. Chromatogram of NAP extracted at 228 nm showing the by-products formed at 6.93, 8.73 and 11.13 min respectively under Solar/MIL-88-A/PS system.....	48
23 Effect of $[NaCl] = 200 - 20,000$ mg L ⁻¹ on the degradation of NAP as function of time (min): (a) in the UVA/ MIL-88-A/PS/NAP system and (b) in the solar/MIL-88-A/PS/NAP system. Experimental conditions $[NAP]_0 = 50$ ppm, $[PS]_0 = 2$ mM, $[MIL-88-A]_0 = 25$ mg L ⁻¹ . Error bars are calculated as <i>tsn</i> where absent bars fall within the symbols.	50
24. Degradation by-products of NAP under chloride effect in Solar/MIL-88-A/PS. Experimental conditions $[NAP]_0 = 50$ ppm, $[PS]_0 = 2$ mM, $[MIL-88-A]_0 = 25$ mg L ⁻¹ , $[NaCl] = 20,000$ mg L ⁻¹	51
25. Effect of different carbonate concentration $[CO_3^{2-}] = 1 - 100$ mM on the degradation of NAP as function of time (min): (a) in the UVA/ MIL-88-A/PS/NAP system and (b) in the solar/MIL-88-A/PS/NAP system. Experimental conditions $[NAP]_0 = 50$ ppm, $[PS]_0 = 2$ mM, $[MIL-88-A]_0 = 25$ mg L ⁻¹ . Error bars are calculated as <i>tsn</i> where absent bars fall within the symbols.	53
26. Degradation by-products of NAP under carbonate effect in Solar/MIL-88-A/PS. Experimental conditions $[NAP]_0 = 50$ ppm, $[PS]_0 = 2$ mM, $[MIL-88-A]_0 = 25$ mg L ⁻¹ , $[CO_3^{2-}] = 100$ mM.	54
27. Effect of different phosphate concentration $[PO_4^{3-}] = 1 - 10$ mM on the degradation of NAP as function of time (min): (a) in the UVA/ MIL-88-A/PS/NAP system and (b) in the	

Solar/MIL-88-A/PS/NAP system. Experimental conditions $[NAP]_0 = 50$ ppm, $[PS]_0 = 2$ mM, $[MIL-88-A]_0 = 25$ mg L ⁻¹ . Error bars are calculated <i>astsn</i> where absent bars fall within the symbols.	56
28. Degradation by-products of NAP under phosphate effect in Solar/MIL-88-A/PS. Experimental conditions $[NAP]_0 = 50$ ppm, $[PS]_0 = 2$ mM, $[MIL-88-A]_0 = 25$ mg L ⁻¹ , $[PO_4^{3-}] = 10$ mM.	57
29. Effect of pH values on the degradation of NAP as function of time (min): (a) in the UVA/ MIL-88-A/PS/NAP system and (b) in the Solar/MIL-88-A/PS/NAP system. Experimental conditions $[NAP]_0 = 50$ ppm, $[PS]_0 = 2$ mM, $[MIL-88-A]_0 = 25$ mg L ⁻¹ . Error bars are calculated <i>astsn</i> where absent bars fall within the symbols.	59
30. Degradation by-products of NAP under pH effect in Solar/MIL-88-A/PS. Experimental conditions $[NAP]_0 = 50$ ppm, $[PS]_0 = 2$ mM, $[MIL-88-A]_0 = 25$ mg L ⁻¹ , pH = 9.	60
31 EPR spectra. Green – simulated EPR spectrum for trapped methyl radicals. $a_N = 1.58$ mT, $a_H = 2.28$ mT. Blue – simulated EPR spectrum for trapped hydroxyl radicals. $a_N = 1.49$ mT, $a_H = 1.49$ mT. Red – the sum of the above two simulated trapped radical spectra. Black – experimental EPR spectrum under the following Experimental conditions: $[PS] = 2.5$ mM, $[MIL-88-A] = 12.5$ mg L ⁻¹ , $[DMPO] = 100$ mM.	63
32 . EPR spectra of DMPO-radical adducts in different reaction systems. Experimental conditions: $[PS] = 2.5$ mM, $[MIL-88-A] = 12.5$ mg L ⁻¹ , $[DMPO] = 100$ mM. The acquisition duration of EPR spectra is about 100 min for all systems.	64
33. HPLC chromatogram at T = 25 °C showing NAP and its byproducts at reaction time t= 100 mins.	65
34. Mass spectrum fragmentation pattern of BP1, BP2 and BP3	66
35. (a) Image of the sum of all positives secondary ions of the MIL-88-A as prepared in the presence of NAP and PS at t = 80 min. The color scale goes from black (lack of emission) to white (saturated emission). (b) Overlay of the characteristic peak of MIL-88-A, Fe ⁺ ion at m/z 56 image (red color) and the characteristic peak of decarboxylated NAP at m/z 185.1 image (green color).	69
36. Activation mechanism of PS in the UVA/MIL-88-A system.	69
37. Overall degradation mechanism of NAP in the UVA/MIL-88-A/PS system.	70

TABLES

Table

1. (a) pH values of the different reaction system during the experiment in the UVA/MIL-88-A/PS/NAP system and (b) pH values of the different reaction system during the experiment in the Solar/MIL-88-A/PS/NAP system	52
2. NAP and byproducts identified by MS.....	68

ABBREVIATIONS

Abbreviation	Meaning	Page
AOPs	Advanced oxidation processes	13
BET	Brunauer–Emmett–Teller	29
BP1	Byproduct one	68
BP2	Byproduct two	68
BP3	Byproduct three	68
DAD	Diode array detector	25
DI	Deionized water	23
DLS	Dynamic light scattering	21
DMPO	5,5-dimethyl-1-pyrroline N-oxide	61
EPR	Electron Paramagnetic Resonance	61
FTIR	Fourier-transform infrared spectroscopy	22
HPLC	High performance liquid chromatography	23
HRs	Hydroxyl radicals	13
MOFs	Metal organic frameworks	14
MS	Mass spectrometry	69
NAP	Naproxen	12
NSAIDs	Nonsteroidal anti-inflammatory drugs	12
PPCPs	Pharmaceutical and personal care products	12
PS	Persulfate	13
PTFE	Polytetrafluoroethylene	21
QTOF	Quadrupole Time of Flight	68
SMX	Sulfamethoxazole	55
SRs	Sulfate radicals	14
TGA	Transient global amnesia	21
TOF-SIMS	Time-of-Flight Secondary Ion Mass Spectrometry	35
UVA	Ultraviolet A-rays	19
WWTPs	Wastewater treatment plants	13
XRD	X-Ray diffraction	21

CHAPTER 1

INTRODUCTION

1.1 PPCPs as emergent contaminants

Pharmaceuticals and personal care products (PPCPs) has raised major concern among scientific and regulatory community during the last three decades, where a sustainable amount of studies has been done to explicate the effects and risks of PPCPs [1]. PPCPs which contain a diverse organic group, such as hormones, antibiotics, NSAIDs, fragrances, etc., have been classified as emerging contaminants due to their possible threats on human health and aquatic environment. Their increased global occurrence was attributed to the increasing human population as well as elevation of life expectancy [2–4]. All these factors contribute to an increase in the quantity and variety of pharmaceuticals ingested and subsequently released into the environment. PPCPs can enter the environment through different routes, where significant quantities are emitted from manufacturing sites and sewage treatments [5,6]. Pharmaceuticals that reaches aquatic environment have been found to alter the physiological processes in fish by binding them to their nuclear receptors which alter molecular mechanisms at transcription and/or translation levels [7,8]. On the other hand, pharmaceuticals can affect humans, causing serious health issues that can't be overcome by medicine [9]. Traditional treatment of waste water proved to be ineffective for the removal of pharmaceutical compounds in water, since organic compounds are very chemically stable [4]. Nonsteroidal anti-inflammatory drugs (NSAIDs) are one major type of these pharmaceuticals such as naproxen, ibuprofen and ketoprofen [4]. They have pKa values

ranging from 4.1 to 4.9, and thus exist as ions at neutral pH surface water, making them more resistant to removal. Then there's biodegradation, which has a high cost, a long sludge age, and a long retention time [10]. These PPCPs are made of two components: excipients and active pharmaceutical ingredients (APIs). APIs were found in waste water plants at quantities ranging from ng L^{-1} to $\mu\text{g L}^{-1}$ [2] in several countries around the world [11–15]. These PPCPs categories have been frequently used because to their inexpensive cost, availability over the counter, and minor side effects. As a result, considerable amounts of these pharmaceuticals and their metabolites enter groundwater, as well as surface and drinking water [16,17].

1.2 Persulfate based AOPs

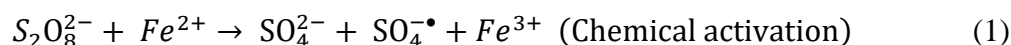
Advanced oxidation processes (AOPs) have recently acquired increasing interest in wastewater treatment technologies development. They have shown efficiency in the elimination of organic compounds that can't be removed by conventional wastewater treatment plants [18]. AOPs are processes that generates reactive species, of the most important hydroxyl radicals (HRs), which degrade rapidly and non-selectively a wide range of organic pollutants in oxidative mechanism [8,9,11]. Common AOPs include UV-based processes (UV/H₂O₂, UV/H₂O₂/O₃, etc.), ozonation, Fenton reaction (Fe²⁺/H₂O₂) and persulfate based AOPs are currently used in industrial WWTPs [21–23].

Activated persulfate oxidation is a newly emerging AOP for degradation of organic pollutants, where persulfate ($E^0 = 2.1 \text{ V}$), upon activation generates a powerful oxidizing agent known as sulfate free radicals ($E^0 = 2.6 \text{ V}$) [12,13]. This technique is environmentally

friendly compared to other chemical process, as they neither transfer contaminates from one phase to another [25].

1.3 Activation techniques

Radical species, mainly sulfate radicals (SRs), can be formed in homogeneous systems via electron transfer by chemical activation of persulfate (Eq. 1) [26,27], photolysis (UV 254nm) (Eq. 2) [28–30], thermolysis (Eq. 3) [31–33], or in heterogeneous systems where chemical activation can be accomplished by using MOFs or magnetite [34,35].



1.4 Metal organic frameworks (MOFs): properties and characteristics

Metal organic framework (MOFs), are a novel class of porous materials, composed of a metal ion or a cluster of metal ions connected to an organic molecule called the linker. In past studies, MOFs were considered as coordination polymers. However, soon it was discovered that the inorganic part possesses larger dimensionality that can form layers and frameworks not only chains [36,37]. MOFs are characterized by their high surface area (10,000 m² /g) and high porosity (0.99 cm³g⁻¹10⁻² for MIL-88-A) [38,39]. These properties

resulted to their use in wide applications such as drug delivery [40,41], magnetism [42], polymerization [43], catalysis [44], and many other applications.

MOFs had been used in the elimination of organic contaminants and dyes from wastewater due to their adsorptive properties [36]. MOFs, containing metals like iron and cobalt have been reported for the activation of PS, as it can be used as a heterogeneous catalyst. In these studies, MOFs like Fe-MOF-74 [45], MIL-53 [46] and MIL-100 [47] were used as photocatalysts for the degradation of dyes. Promising experimental results were established in recyclability and reproducibility rendering MOFs as greener alternative [48].

1.5 MOFs in adsorption and catalysis

MOFs that are a combination of Ti, Zr, Fe, Al and/or Cr with carboxylate-based ligands are mainly stable in water and have been often used for their adsorptive properties towards hazardous organic compound in waste water [28,41–43]. For example, Tong et al. studied the removal of methylene blue (MB), a toxic cationic dye from aqueous solution using MIL-100-Cr. Good adsorption capacity (211.8 mg/g) was shown in the results [52], but it presents several drawbacks, one of them is chromium, which is a toxic metal especially in its hexavalent state [53]. Furthermore, MIL-100 was synthesized using hydrofluoric acid, which is very hazardous and corrosive and should not be used in environmental applications [54]. MIL-100-Fe has been employed in a variety of adsorption applications for the removal of methylene orange (MO), naproxen and bisphenol A [52,55,56]. All the above studies show that adsorption alone is not sufficient to remove the trace amounts of PPCPs mentioned. In

addition to adsorption, MOFs, especially MOFs that contain Fe as a metal ion, proved to have effective photocatalytic effect in removing organic contaminants. Roy et al studied the degradation of Bisphenol A by activating PS using MIL-88A(Fe)/MoS₂, where MIL-88A(Fe)/MoS₂ shows a good catalytic potential in activating PS to degrade BPA [57]. As proposed in their research, as well as other studies employing iron-based MOFs, the mechanism of photo-catalysis reaction is based on transformation of Fe (III) into Fe (II) (eq. 4), which then transform PS into sulfate radicals (Eq.3), allowing the degradation process to occur by free radical mechanism (Eq.5) as in the following reactions [58] .



Fe-MOF-74@SiO₂ was used by Ding et al. for the degradation of dimethyl phthalate (DMP) in water. Results showed that DMP achieve complete elimination in 60 min under optimal conditions [59]. Moreover, cobalt-based MOF was used for dibutyl phthalate (DBP) degradation by activating peroxymonosulfate (PMS). The recyclability of MOF was also established for five times, with no significant reduction in the rate of [DBP] degradation [60]. Nonetheless, because Co is a toxic heavy metal, its use may be harmful to both human health and the quality of the established environmental systems [15]. Iron based MIL-88-A was used by Wang et al. to activate persulfate for effective degradation of OG [61]. MIL 88-A was shown to be an effective recyclable heterogeneous catalyst for degrading OG in water.

1.6 Naproxen as a target/model molecule

Non-steroidal anti-inflammatory drugs (NSAIDs) and antibiotics are the most detected among pharmaceuticals in the environment. NSAIDs have been widely used in human medication due to their low cost, absence of addictive side effect and availability [62]. As they were found in surface water in increasing concentrations (ng/L to $\mu\text{g/L}$) [63]. Naproxen (NAP), is the most used NSAID with antipyretic and analgesic properties. To enhance solubility, NAP is frequently provided as a sodium salt. NAP toxicity was reported on humans not only on bacteria and microcrustaceans, which are diverse arthropod taxon which includes such animals as crabs, lobsters, crayfish, shrimp. Reports also showed that people who consume trace amount for a long period of time may have higher risk of having stroke or heart attack [62]. Many studies have been conducted over the past years on elimination of NAP from waste water by photo-degradation, ozonation, ultra-sonication, gamma irradiation, nanofiltration [64]. The mentioned treatment methods were energy consuming, leading to toxic metabolites. For example, Ghauch et al demonstrates the elimination of NAP by thermally activated persulfate [64]. Results shows that the thermal activation of PS is an efficient way for NAP total degradation. However, this system is not recyclable or reproducible. Accordingly, PS will be activated using a heterogeneous catalyst (MIL-88-A).

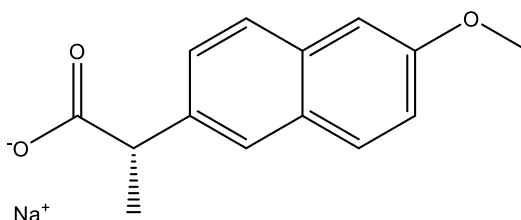


Fig. 1. Chemical structure of Naproxen.

1.7 The choice of MIL-88-A in the study

The choice of MOF for our study was based on several factors. It had to contain an activator metal for persulfate (PS), where iron is considered one of the most proper metals for PS activation, since it is abundant, safe, easy to produce and affordable. Another factor, is the ligand, the MOF's second component, following similar criteria such as safety, affordability and abundance. MIL-88-A fits the required factors where it is composed of ferric chloride as a metal and fumaric acid as a ligand. As for the synthesis, it is a water-based synthesis, contrary to other MOFs that requires organic-based synthesis [45,65].

And we tried to find a green synthesis method which is based on water as a solvent and not an organic solvent and low-cost ligand which is fumaric acid. According to Wan et al. study, the catalytic activity of MIL-88-A with PS in the degradation of orange G (OG) gave the highest degradation rate. MIL-88-A was synthesized at 85°C for two hours.

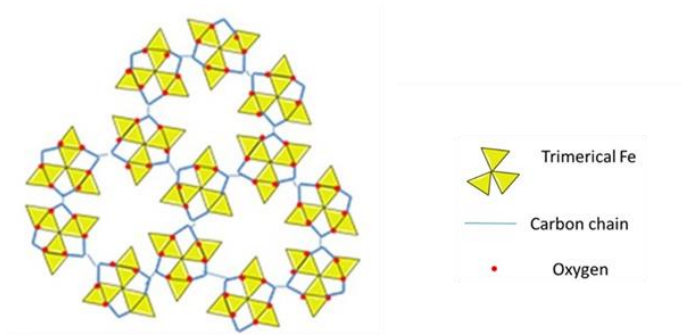


Fig. 2. Illustration of MIL-88-A structure

1.8 Objective

In this study, we attempted to identify other factors that could improve MIL-88-A's characteristics in aqueous solutions and allow it to function as a PS activator in a heterogeneous medium, with the possibility of a synergistic impact. In the two systems UVA/MIL-88-A/PS and Solar/MIL-88-A/PS we observed the effect of NAP elimination in terms of degradation rate, degradation products nature and persistence using Time of Flight high resolution mass spectroscopy (HPLC/QTOF). The two systems will be compared in terms of efficiency and effect of several matrices. The matrices to be considered include pH values, [sulfates], [chlorides] and [nitrates].

CHAPTER 2

MATERIALS AND METHODS

2.1. Chemicals

Naproxen sodium (NAP) ($C_{14}H_{13}NaO_3$) was obtained from Sigma Aldrich (USA), sodium persulfate (PS) ($Na_2S_2O_8$, purity $\geq 99\%$). Potassium iodide (KI) (puriss, 99.0-100.5%) used for PS quantification and phosphate buffer monobasic (H_2NaO_4P assay $\geq 99.0\%$) and dibasic ($HNaO_4P$ assay: 98-100.5%) used to study the effect of phosphate were purchased from Sigma-Aldrich (China, France, and Germany, respectively). Fumaric acid (C_4H_4O) and iron (III) chloride ($FeCl_3$) (both reagent grade $>97\%$) used in the synthesis of MIL-88-A were acquired from Sigma-Aldrich (France and Switzerland respectively). Ethanol (absolute) was purchased from Scharlau (Spain). Formic acid and acetonitrile used as HPLC mobile phase were acquired from Loba Chemie (India) and Honeywell (Germany) respectively. Millipore deionized water (DI) was used in the preparation of all solutions. To evaluate the matrix effect, sodium bicarbonate ($NaHCO_3$) and sodium chloride ($NaCl$) were acquired from Fluka (Netherlands). Furthermore, hydrochloric acid (HCl) and sodium hydroxide used to modify the pH were purchased from Fluka (Switzerland, Germany, respectively).

2.2. Synthesis of MIL-88-A

MIL-88-A Synthesis was done using hydrothermal techniques [35,39,66], where 1,949 mg of fumaric acid and 4,544 mg of ferric chloride were added to a beaker filled with 84 mL of DI water. Then the mixture was stirred for 1 hour using a magnetic stirrer at 450 rpm to homogenize the solution. Later it was transferred into a 100 mL PTFE-lined stainless-steel autoclave and heated at 85°C for 24 hours. The autoclave is left to cool to room temperature after being removed from the oven. The solid formed was then collected and washed with 1:1 of ethanol and DI in a beaker and left for 2 hours. Then it was recovered each time by centrifugation at 4000 rpm (G-force = 2200) for 10 minutes. Washing with ethanol and DI was repeated 3 times, similarly washing with DI alone. The precipitate obtained was then dried in a vacuum oven at 100 °C for 24 hours yielding $2,350 \pm 220$ mg of pure MIL-88-A powder.

2.3.Characterization of MIL-88-A

Characterization of MIL-88-A was done by common techniques reported in literature [61]. A D8 Advance (Bruker) X-ray diffraction pattern (XRD) was used to determine the powder X-ray diffraction pattern of MIL-88-A and guarantee the crystallinity of the crystals. MIL-88-A powder was set on a background zero holder and scanned with a scanning rate of 0.02° per second from 5° to 20° (2 Θ). A scanning electron microscope (SEM), Tescan, Mira III was used to determine the morphology of the synthesized material. The Brunauer-Emmet-Teller surface area and pore size analyzer (Micromeritics, 3 flex surface area characterization) was used to determine the specific surface area and pore size of MIL-88-A.

A Micromeritics, Q2000 dynamic light scattering instrument (DLS) was used to calculate the hydrodynamic diameter, particle size distribution and zeta potential. Thermogravimetric analysis (TGA) of MIL-88-A was performed under nitrogen atmosphere with a heating rate of $5^{\circ}\text{C min}^{-1}$ and a temperature ranging from 30 to 900°C using a TG 209 F1 Iris (Netzsch, Germany). Finally, the Fourier Transform Infrared Spectroscopy (FTIR) of the TGA analyzer exhaust under nitrogen was determined using a Bruker Tensor 27 IR. The XPS measurements were carried out on a Thermo Fisher Scientific VG ESCALAB 220iXL spectrometer, which used focused mono-chromatized Al $K\alpha$ radiation (1486.6 eV) with a beam size of $\sim 500\ \mu\text{m}^2$ (power of 150 W). The measurements were performed on MOF crystals that had been combined with 10% conductive carbon (Super-C 65, Timcal). The pressure in the analytical chamber was about $2 \times 10^{-9}\text{ mbar}$. On a clean silver surface, the spectrometer was calibrated by measuring the $\text{Ag}3d_{5/2}$ peak with a binding energy (BE) of 368.25 eV and a full width at half maximum (FWHM) of 0.78 eV . All spectra were acquired at 30 eV pass energy and 50 eV for the surveys, in steps of 50 meV and with a dwell time of 50 ms . The binding energy peak sites are calibrated using the C1s at 284.6 eV .

2.4. Experimental conditions and procedure

Solutions were prepared using DI on a daily basis. NAP stock solution (100 ppm) was prepared by dissolving 100 mg of naproxen sodium in 1L volumetric flask and kept on a magnetic stirrer overnight away from the light. PS stock solution (100 mM) was prepared by dissolving 2.381 mg in 100 mL volumetric flask.

For the experiments that were conducted in the presence of UVA in the laboratory, the required volume of NAP stock solution was added with the corresponding amount of deionized water (DI) to a 110 mL homemade watertight borosilicate recipient that contains the essential amount of MIL-88-A. It was attached radially to a labquake shaker rotisserie of speed 8 revolutions/min and left stirring for a period of 1 hour to reach equilibrium adsorption. Thereafter the medium was spiked with the required volume of PS stock solution, where continuous stirring was maintained to ensure uniform mixing. 1.5 mL samples were collected 30 seconds before and after the addition of MIL-88-A as well as before the addition of PS and every 20 mins for the next 1 hour and 40 minutes, where the reaction time was set to be 2 hours and 40 minutes. All samples were filtered using a 0.45 μm PTFE 13 mm disc filters (Jaytee Biosciences Ltd., UK) and stored in amber HPLC vials at 4°C prior to analysis.

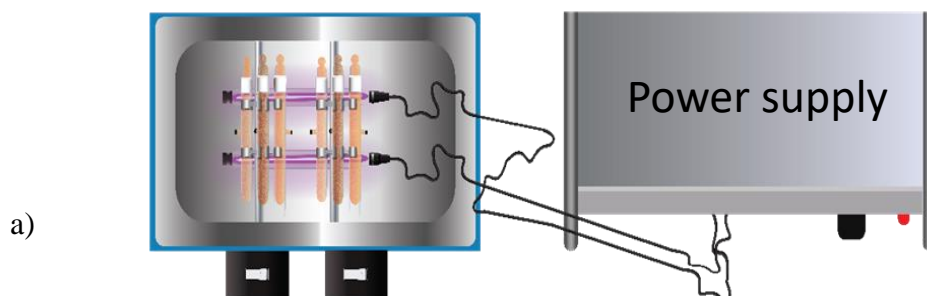
For experiments that were carried out under solar irradiation, the required volume of NAP stock solution was added with the corresponding amount of DI to a 110 mL homemade watertight borosilicate that contains the essential amount of MIL-88-A, it was attached to radially to a labquake shaker rotisserie of speed 8 revolutions/min. left stirring in dark for a period of 1 hour to reach equilibrium adsorption, then the medium is spiked required volume of PS stock solution, where continuous stirring was maintained to ensure uniform mixing and

moved to be in sunlight. 1.5 mL samples were collected 30 seconds before and after the addition of MIL-88-A as well as before the addition of PS and every 5 mins for the next 25 mins then every 10 mins till 125 mins, where the reaction time was set to be around 2 hours. Sample collection timing was varied by different experiment requirements.

Control experiments were carried either in the absence of PS and/or MIL-88-A and/or UV. All experiments were performed in triplicates and each sample was analysed twice for uncertainty determination.

2.5.Reaction setup

To investigate the activation of PS by photo-activated MIL-88-A for the degradation of NAP, reactions take place in 110 mL homemade watertight borosilicate that were attached radially to a labquake shaker rotisserie of speed 8 revolutions/min. Reactors were placed in a stainless-steel reflector with 2 commercial T5 8 watts near-ultraviolet (UVA) fluorescent lamps that were placed under the reactors (Fig. 3a). Similarly, for solar system, UV lamps were removed and irradiation relied only on solar beam without the use of any sunlight concentrator (Fig. 3b).



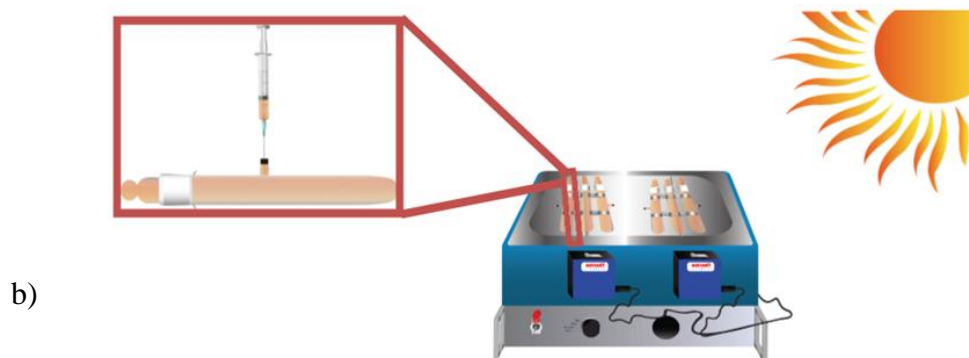


Fig. 3. Experimental Setup of a) MIL-88-A/PS/UVA/NAP and b) MIL-88-A/PS/Solar/NAP systems

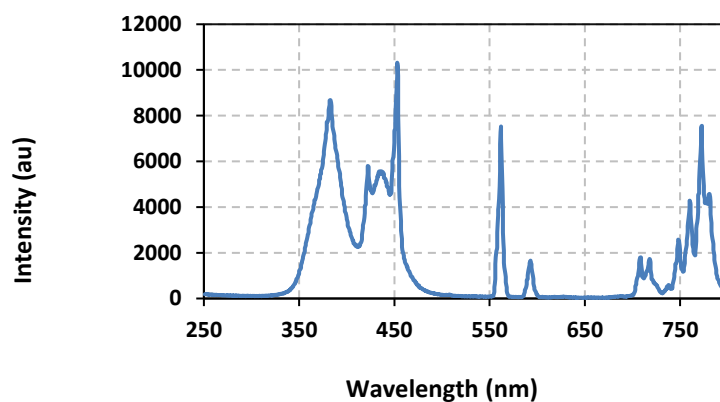


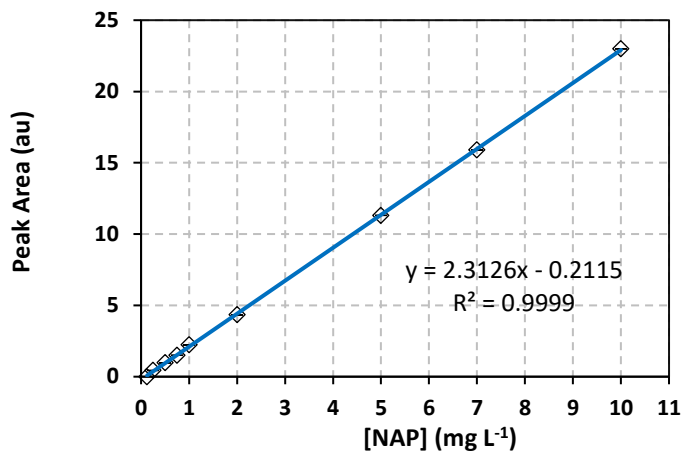
Fig. 4. Emission spectrum of the UVA mosquito lamps used in the experiment

2.6. Chemical analysis

NAP analysis was performed on a high-performance liquid chromatography (HPLC) equipped with a quaternary pump, a vacuum degasser, an autosampler unit with cooling maintained at a temperature of 4°C, and a thermally controlled column compartment set at temperature of 30°C. A C-18 reverse phase column (5 μm ; 4.6 mm internal diameter x 250

mm in length) connected to a security guard column HS C-18 (5 μm ; 4.0 mm internal diameter 20 mm long) connected to a guard column, and a DAD (diode-array detector). The mobile phases consisted of 0.1% (v/v) formic acid (45%) and acetonitrile (55%) under a flow rate 1mL/min and injection volume 10 μL , all under isocratic mode. Naproxen was eluted at a retention time of 7.6 min. It was detected at λ of 228 nm. The linear dynamic range (LDR) obtained was between 0.1 and 10 mg L^{-1} with limit of detection = 0.0009 mg L^{-1} as it appears in Fig. 5. According to the methods developed by Baalbaki et al [67].

a)



b)

Linest Output NAP			
y = mx + b			
m	2.312642	-0.21149	b
s _m	0.008292	0.037073	s _b
R ²	0.99991	0.083388	s _y

Fig. 5. (a) Calibration curve of NAP. The error bars are calculated at 95% confidence level. Absorbance = $A(\text{mean}) \pm \frac{ts}{\sqrt{n}}$, where t is the student value ($t = 2.447$ for 6 degrees of freedom at 95% confidence level) and s the standard deviation of 7 replicates. (b) The LINEST output calculated through Excel provided the slope, y intercept, the regression coefficient and all statistical data including standard deviations on variables.

CHAPTER 3

RESULTS AND DISCUSSION

3.1. Characterization of MIL-88-A

3.1.1. XRD pattern of MIL-88-A

MIL-88-A XRD diffraction patterns showed well-defined peaks at 2θ positions of 7.7° , 10.6° and 12.9° (Fig. 6). Although not exactly like those reported in literature [35,61], but these peaks are consistent with the theoretical simulated ones, indicating the successful synthesis of MIL-88-A.

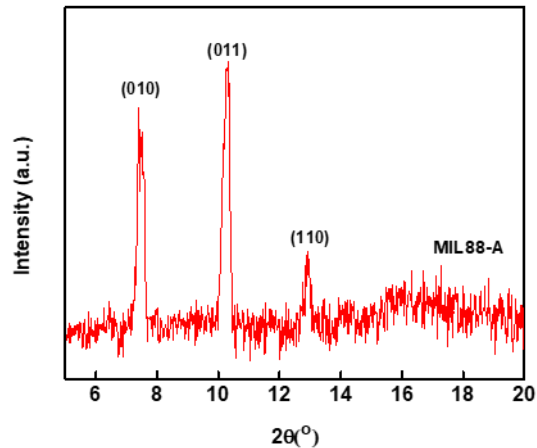


Fig. 6. XRD diffraction pattern of MIL-88-A

3.1.2. SEM images of MIL-88-A

SEM images shows MIL-88-A crystals that exhibit hexagonal rod-like morphology. This also agrees with the reported morphology of MIL-88-A in literature [35,61]. The rod-like crystals are in nanometer-scale, with the size ranging from 100 to 800 nm as shown in Fig. 7. This was proved by dynamic light scattering analysis that shows an average hydrodynamic diameter of 411 nm with the distribution profile of the hydrodynamic diameter showed in Fig.7 and zeta potential analysis was performed in deionized water matrix. The values obtained ranged from -5 mV to +5 mV, recommending that MIL-88-A crystals require sustained stirring in order to remain suspended because they are susceptible to settling.

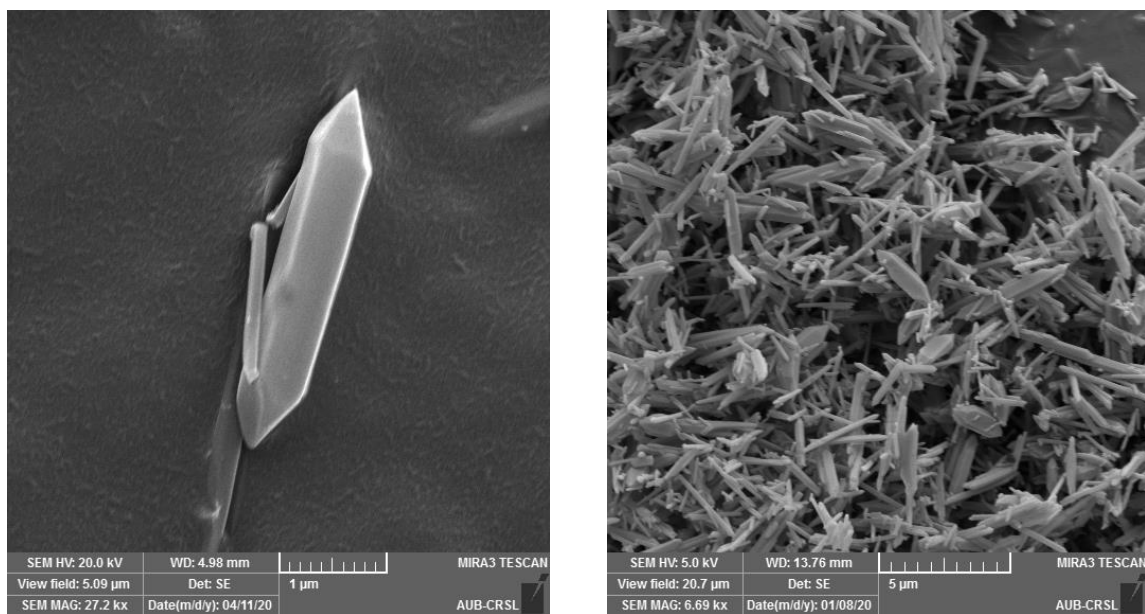


Fig. 7. SEM of crystals of MIL-88-A at different magnifications

3.1.3. BET analysis of MIL-88-A

BET analysis showed a good desorption and adsorption phenomena as shown in isotherms of Fig. 8 and the calculated surface area of MIL-88-A was $37.3 \text{ m}^2/\text{g}$, which is slightly higher to that reported in literature ($< 30 \text{ m}^2/\text{g}$) [61].

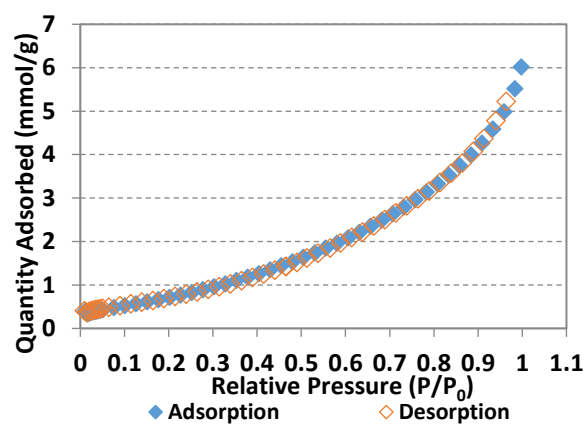


Fig. 8. BET adsorption/desorption isotherms of MIL-88-A [68]

3.1.4. TGA and FTIR analysis of MIL-88-A

The TGA analysis (Fig. 9) showed a 6 % weight reduction at furnace temperature under 100 °C. This is generally because of water evaporation from the MIL-88-A sample. Then, at that point, a second weight loss (14.7%) was noticed and referred to the separation of the organic linker (fumaric acid) that is used in the synthesis process of the MIL-88-A sample, which continued till 400 °C, where a huge weight reduction of 30% is distinguished, after which a total breakdown of fumaric acid is seen at around 600 °C bringing about a last weight reduction of 14% before ash remains. At around 300°C, a different pattern of total dissociation was observed with pure fumaric acid, as previously reported in the literature [69]. It is proposed that when fumaric acid is entrapped within the MIL-88-A framework, its thermal stability increases, necessitating a higher temperature for dissociation, which was then validated by FTIR analysis (Fig. 10). At three different temperatures (316, 445, and 613 °C), the results revealed three significant signals. In fact, the observed spectra revealed bands resembling the following functional groups: (i) O = C = O stretching at 2350 cm⁻¹ at all temperatures; (ii) C = C = O stretching at 2100–2150 cm⁻¹ at temperature 613 °C confirming the existence of fumaric acid residues at $t \geq 300$ °C.

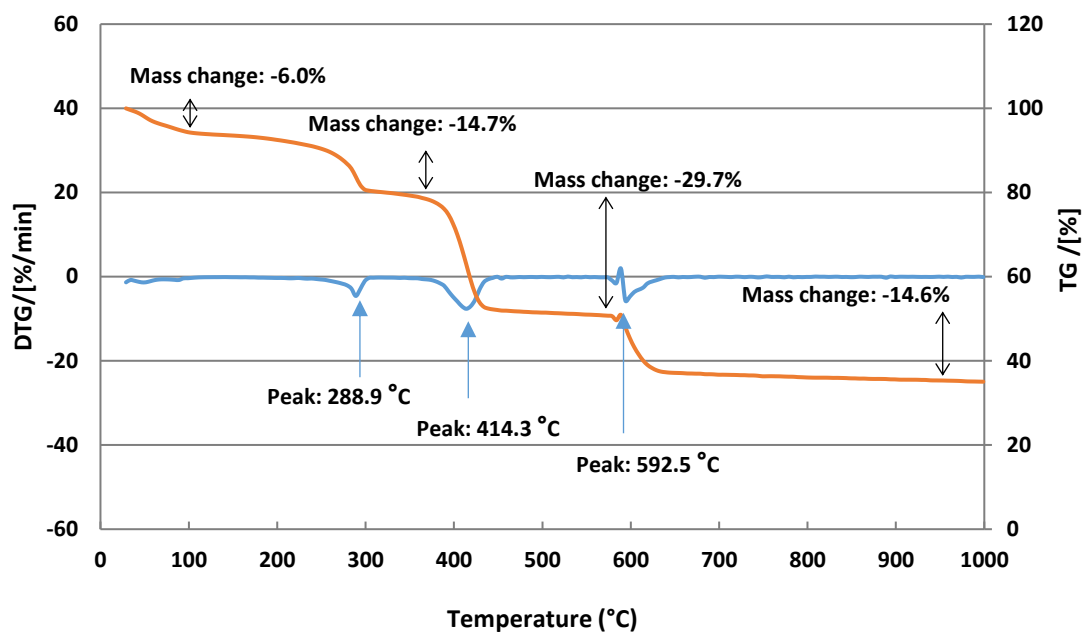


Fig. 9. TGA analysis of MIL-88-A [68]

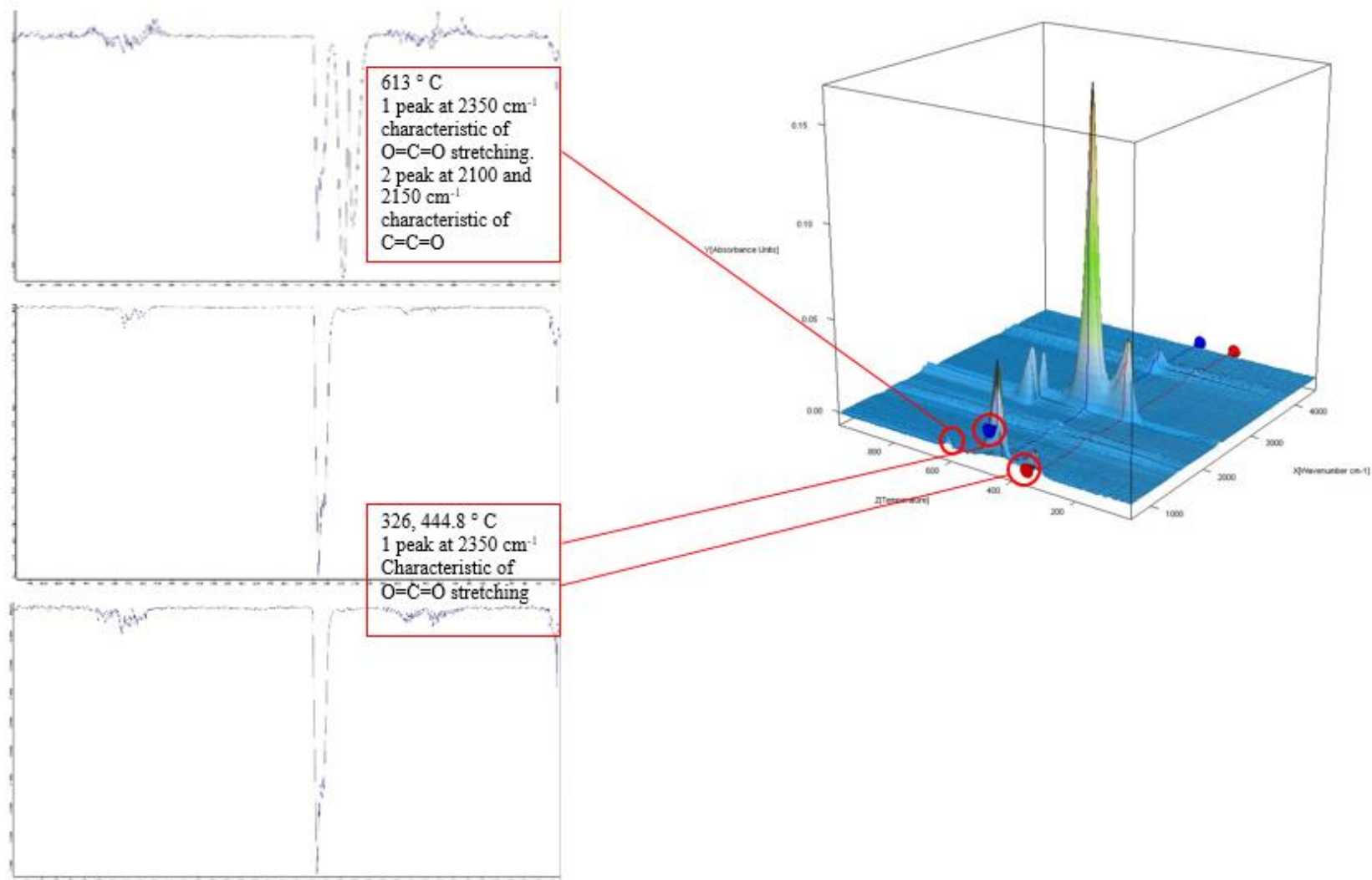


Fig. 10. TGA-FTIR analysis of the synthesized MIL-88-A [68]

3.1.5. XPS analysis of MIL-88-A

MIL-88-A XPS analysis was performed before and after the experiment, as can be observed from Fig. 11. XPS was used to examine the oxidation state of the Fe within the MOF powders on the three prepared samples (as synthesized, after experience without UV, and after experience with UV). The Fe $2p_{3/2-1/2}$ and O 1s core levels are shown to have the same features, confirming that the oxidation state of the Fe remains the same after the experience. The Fe $2p_{3/2}$ and Fe $2p_{1/2}$ binding energy are measured at 712.4 eV and 726 eV respectively. The binding energy position as well as the presence of a satellite peak at 719.4 eV are characteristic of Fe in oxidation state of +3 like in Fe_2O_3 .

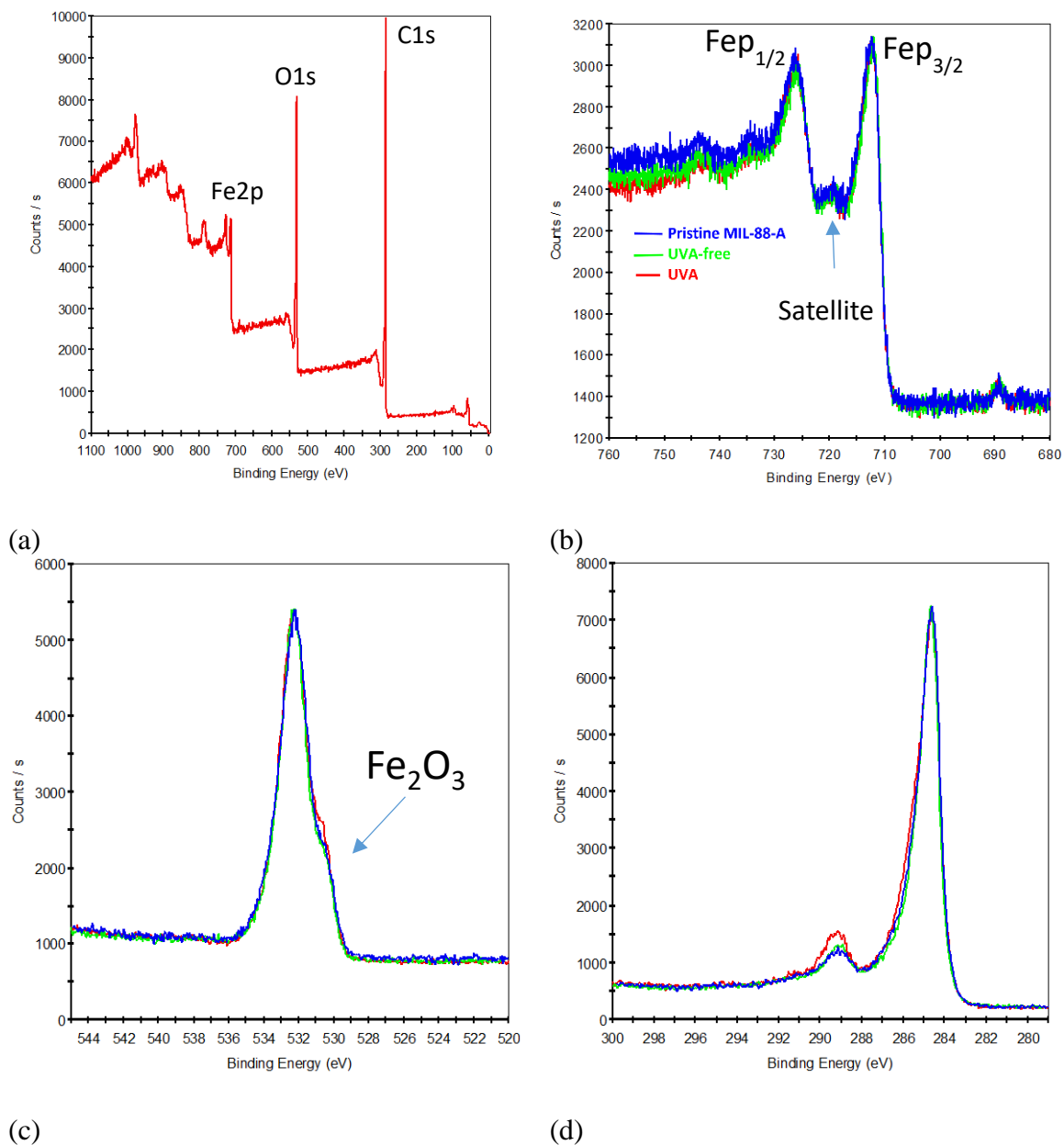


Fig. 11. XPS analysis of pristine MIL-88-A and used MIL-88-A in UVA-free and UVA-irradiated systems after the oxidation reaction. (a) XPS survey spectra, (b) Fe_{2p_{3/2-1/2}} spectra, (c) O1s spectra and (d) C1s spectra. XPS spectra of all samples are almost overlap

3.1.6. TOF SIMS technique

The TOF SIMS technique was used to characterize pure MIL-88-A that had been synthesized without the adsorption of any organic pollutants. As shown in Fig. 12, the mass spectrum contained several ions corresponding to many fragments, including $[C_3H_5]^+$, $[Fe]^+$, $[Fe_2O]^+$, $[C_8H_5O_3]^+$, $[Fe_3O_2]^+$, and $[Fe_3O_3H]^+$ at 41, 56, 127.9, 149, 199.8, and 217.8 m/z. Those ions are attributed to secondary ions (single and recombined) produced by MIL-88-A constituents such as iron chloride and fumaric acid under Bi^{3+} cluster beam impact. By the end of the experiment at room temperature, iron leaching from MIL-88-A showed insignificant concentrations (e.g., $16 \mu g L^{-1}$). This very low value affirms to the solid material's good stability ($[MIL-88-A]_0 = 25 mg L^{-1}$) even in an oxidative medium following PS spiking (5 mM) of the NAP solution ($50 mg L^{-1}$) and after 2 h of reaction.

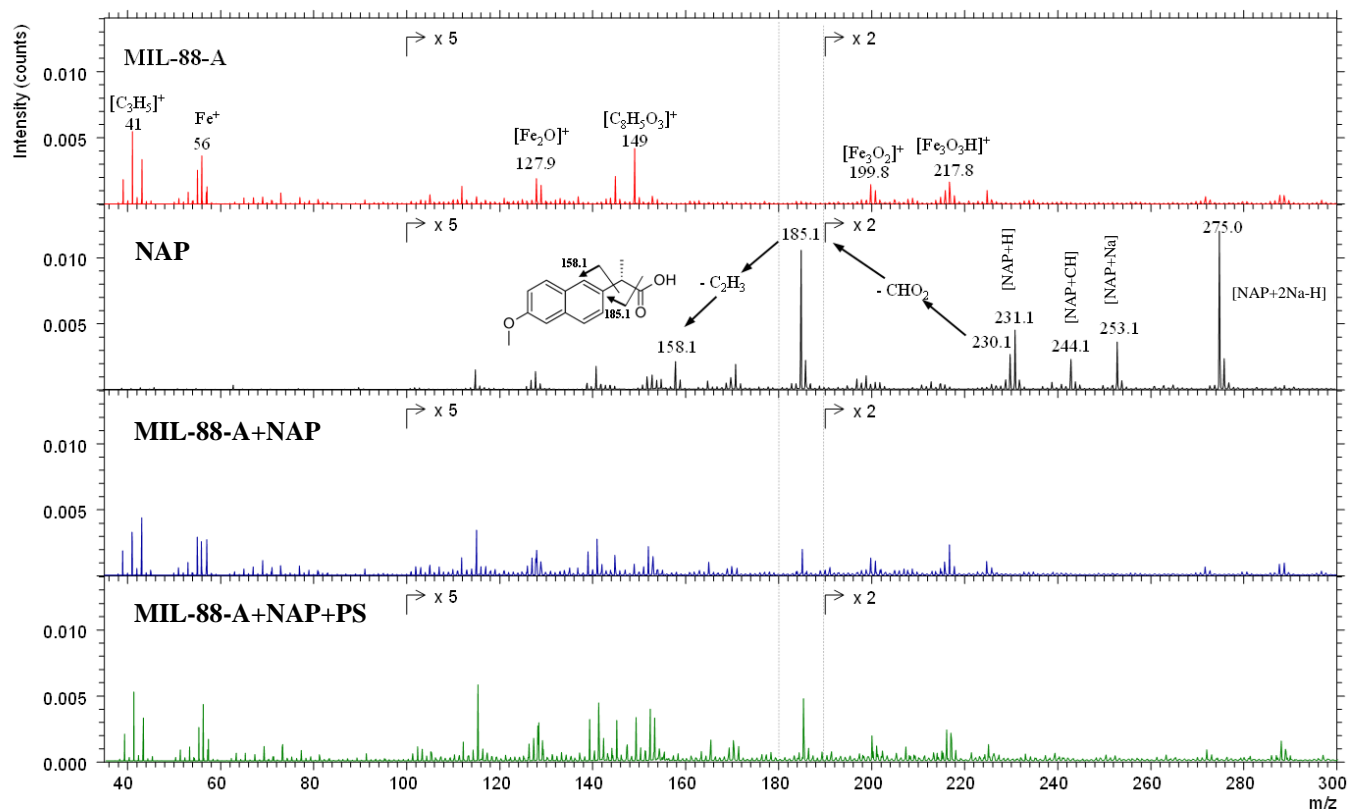


Fig. 12. TOF-SIMS positive spectra of (a) MIL-88-A as prepared, (b) NAP powder, (c) MIL-88-A after use in the presence of NAP and (d) MIL-88-A after use in the presence of NAP and PS. The spectra are normalized to the Bi_3^+ received dose and have the same y axis scale. Areas of the spectra are multiplied by 5 or by 2 for visual purposes.

3.2.MIL-88-A/PS system controls

Control experiments were conducted to study the activation of PS by MIL-88-A in the absence and in the presence of either UVA lamps or sunlight. In a 100 mL solution containing $[NAP]_0 = 50$ ppm, 25 mg L^{-1} of $[MIL-88-A]_0$ was added and left stirring for a period of 1 hour to reach equilibrium adsorption, then the medium is spiked with $[PS] = 2$ mM, where continuous stirring was maintained to ensure uniform mixing. 1.5 mL samples were collected 30 seconds before and after the addition of MIL-88-A as well as before the addition of PS and every 20 mins for the next 1 hour and 40 minutes, where the reaction time was set to be 2 hours and 40 minutes. NAP degradation was tested in the absence and in the presence of either UV or solar irradiation. As it can be noticed, in MIL-88-A/PS system, the drop of $[NAP]$ after 60 mins from spiking persulfate was 11.6%. In UVA/MIL-88-A/PS and Solar/MIL-88-A/PS system the % degradation increase to 87.2% and 99.8%, respectively. This shows the significant effect of UVA and solar on NAP degradation.

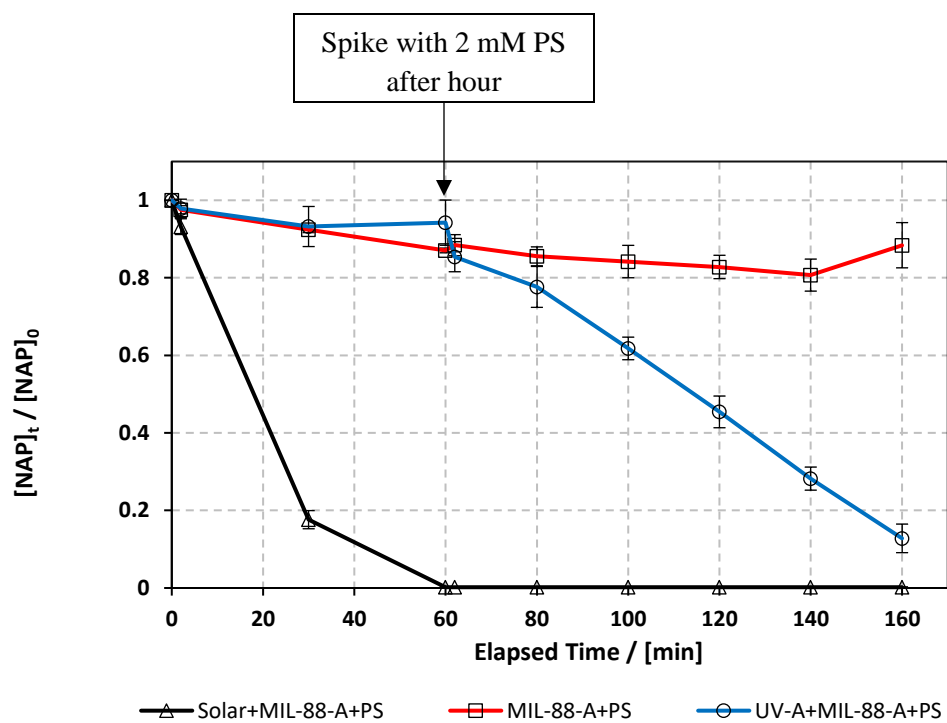


Fig. 13. Elimination of NAP in a combined MIL-88-A/PS system and in the presence of MIL-88-A only and PS only under UVA light. Experimental conditions: $[\text{NAP}]_0 = 50 \text{ ppm}$, $[\text{PS}]_0 = 2 \text{ mM}$, $[\text{MIL-88-A}]_0 = 25 \text{ mg L}^{-1}$. Error bars are calculated as $\frac{ts}{\sqrt{n}}$, where absent bars fall within the symbols.

3.3.UVA/MIL-88-A/PS system

Preliminary experiment was done to study the effect of UVA on NAP degradation. In a 100 ml solution containing $[\text{NAP}]_0 = 50$ ppm, 25 mg L^{-1} of $[\text{MIL-88-A}]_0$ was added and left stirring for a period of 1 hour to reach equilibrium adsorption, then the medium is spiked with $[\text{PS}] = 2$ mM, where continuous stirring was maintained to ensure uniform mixing. 1.5 mL samples were collected 30 seconds before and after the addition of MIL-88-A as well as before the addition of PS and every 20 mins for the next 1 hour and 40 minutes, where the reaction time was set to be 2 hours and 40 minutes. Control experiments were also conducted, where NAP degradation was tested in the presence of PS only and MOF only under the mentioned conditions. In MIL-88-A only and PS only, the drop in $[\text{NAP}]$ after 60 mins from spiking with PS was 19.25% and 51.31% respectively. The % degradation increases to 87.2% when MIL-88-A and PS are combined. This shows the effectiveness of MIL-88-A/PS/UVA system in the elimination of NAP as shown in Fig. 14.

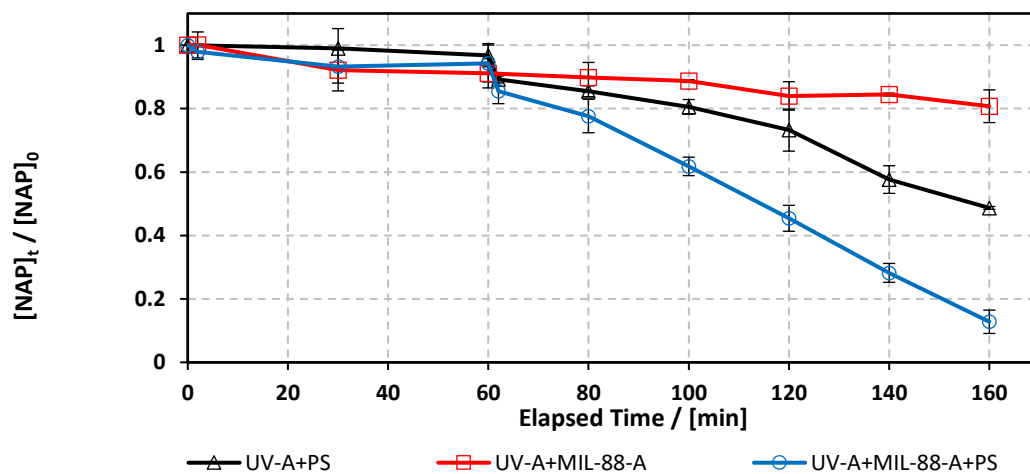


Fig. 14. The % degradation of NAP irradiated with UVA lamps as function of time (min) in three reactions under different conditions: PS only, MIL-88-A only, and MIL-88-A with PS. Reactors were irradiated by the UVA lamps placed on the side. Experimental conditions: $[NAP]_0 = 50$ ppm, $[PS]_0 = 2$ mM, $[MIL-88-A]_0 = 25$ mg L⁻¹. Error bars are calculated as $\frac{ts}{\sqrt{n}}$, where absent bars fall within the symbols.

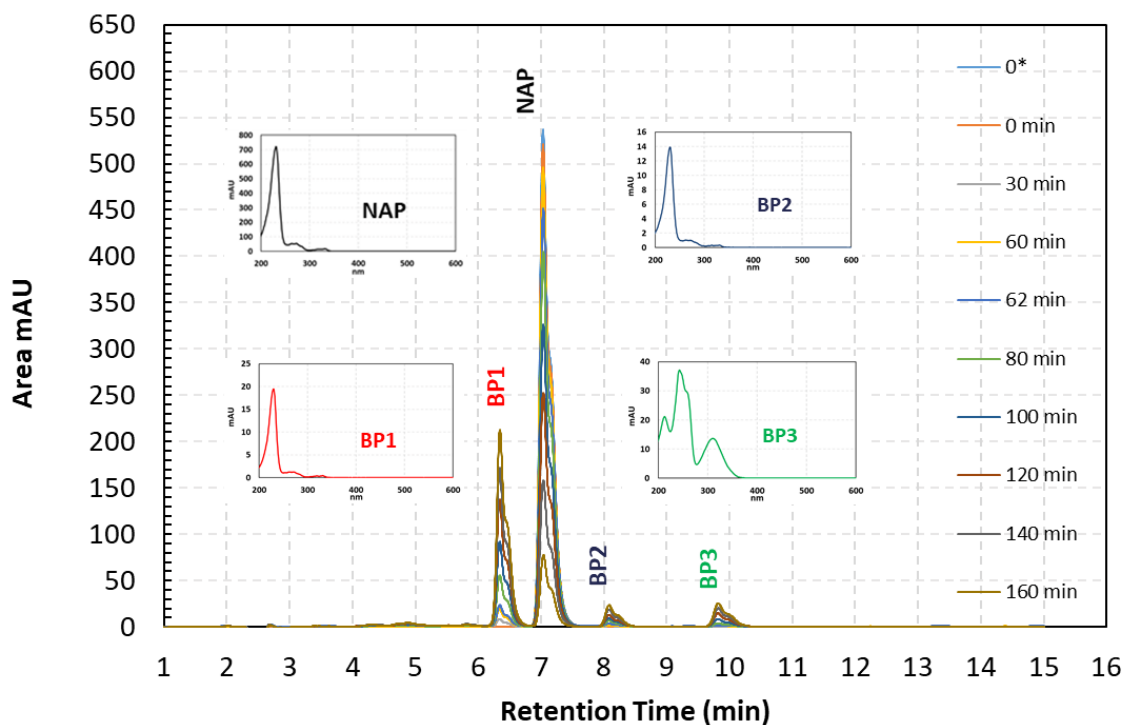


Fig. 15. Chromatogram of NAP extracted at 228 nm showing the by-products formed at 6.30, 8.06 and 9.79 min, respectively under UVA irradiation in UVA/MIL-88-A/PS system.

3.3.1. Effect of NAP dosage

Figure 16 show the effect of different NAP dosage (25-75 ppm) on NAP degradation in UVA/MIL-88-A/PS system. In a 100 mL solution containing [NAP], 25 mg L⁻¹ of [MIL-88-A]₀ was added and left stirring for a period of 1 hour to reach equilibrium adsorption, then the medium is spiked with [PS]₀ = 2 mM, where continuous stirring was maintained to ensure uniform mixing. As NAP concentration was increased from 25 ppm to 75 ppm the % degradation from 99.65% to 77.68%. When the initial NAP concentration was lower, the radical formation rate was greater than the NAP degradation rate, resulting in higher NAP elimination. When the initial NAP concentration increased, insufficient oxidative radicals were used up, resulting in lower NAP removal.

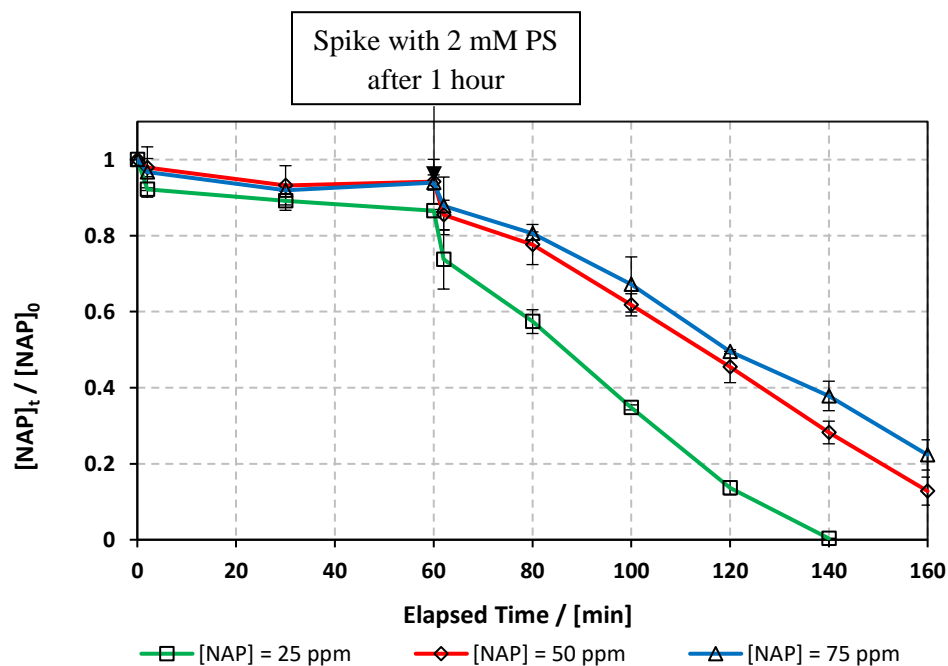


Fig. 16. Effect of NAP concentration on NAP degradation. Experimental conditions: [PS]₀ = 2 mM, [MIL-88-A]₀ = 25 mg L⁻¹. Error bars are calculated as $\frac{ts}{\sqrt{n}}$, where absent bars fall within the symbols.

3.3.2. *Recyclability*

Recyclability is a fundamental parameter when analysing heterogeneous catalysis applications since the catalyst can be recovered and reused. An experiment was conducted, where MIL-88-A was recovered in two successive cycles. The recovery process included separation using centrifugation followed by drying via vacuum oven at 90°C for 24 hours. Recovered MIL-88-A quantity decreases after each cycle, some MIL-88-A crystals get stuck in the 0.45 μm PTFE filter used in the sampling process, causing difficulty in collecting MIL-88-A. The degradation of NAP was reduced after each cycle. For every subsequent cycle, the volume of NAP solution (50 ppm) was adjusted so that the concentration of MIL-88-A remained constant at 25 mg/L, in order to conduct a comparative analysis of the results collected from each cycle. The decrease in efficiency observed after the second cycle may be due to full occupation of the activation sites of MIL-88-A. The % degradation decreases from 87% to 68% and 69% in cycle 2 and 3 respectively. SEM images of MIL-88-A taken after recycling showed that rod-like morphology of MIL-88-A crystals was identical to that of freshly synthesized MIL-88-A, but the homogeneity of MIL-88-A crystals was lost when the crystals were extended. The XRD diffraction pattern of MIL-88-A is similar to that of MIL-88-A initially synthesized, however the intensity of the peaks differs. The BET of MIL-88-A after reaction shows a decrease in the surface area from 37.3 m^2/g to 10.1 m^2/g , confirming the adsorption of NAP on MIL-88-A.

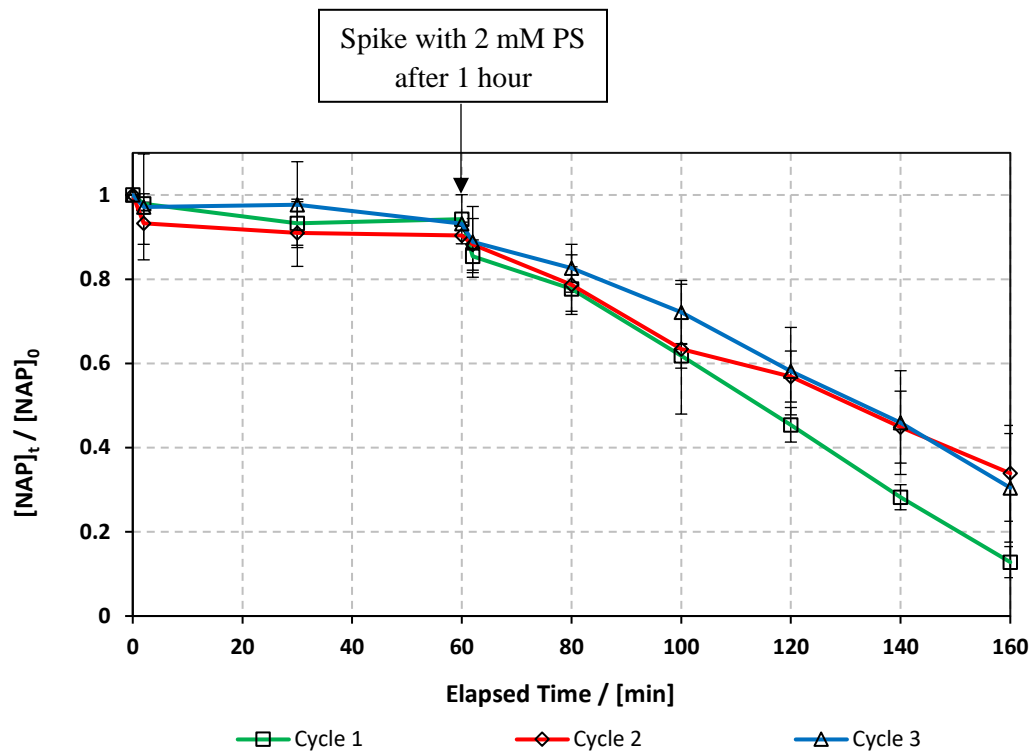
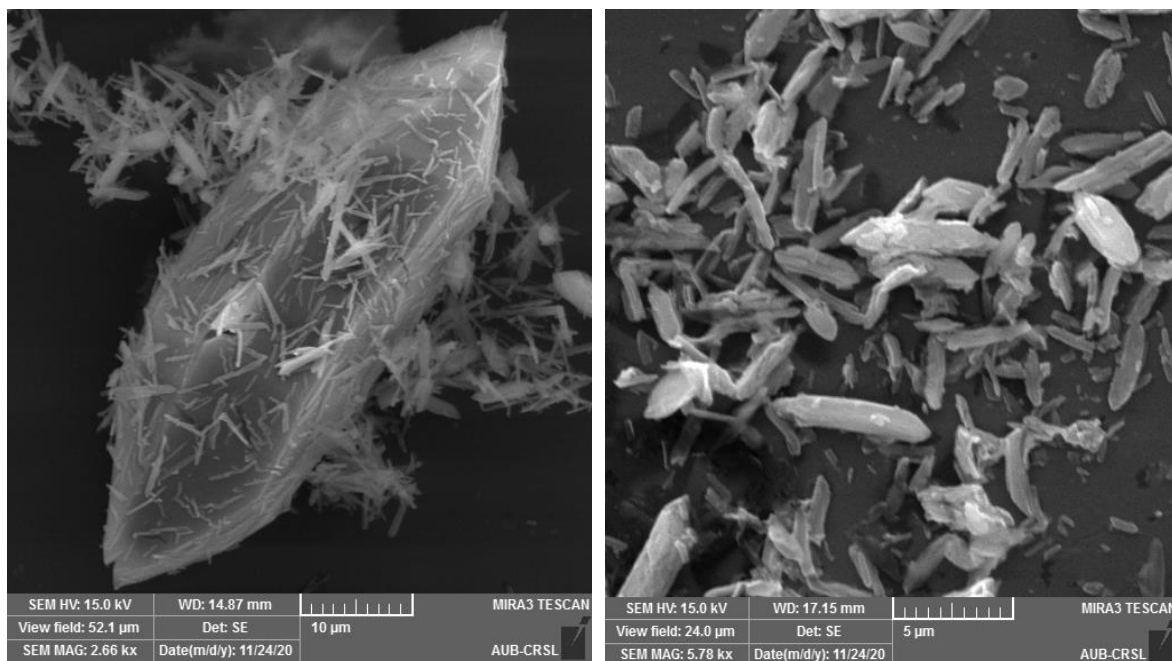


Fig. 17. Recyclability experiments of MIL-88-A in the UVA reactors. $[\text{NAP}]_0 = 50 \text{ mg L}^{-1}$. $[\text{PS}]_0 = 2 \text{ mM}$, $[\text{MIL-88-A}]_0 = 25 \text{ mg L}^{-1}$. Error bars are calculated as $\frac{ts}{\sqrt{n}}$, where absent bars fall within the symbols.



(a)

(b)

Fig. 18. SEM images of recycled MIL-88-A

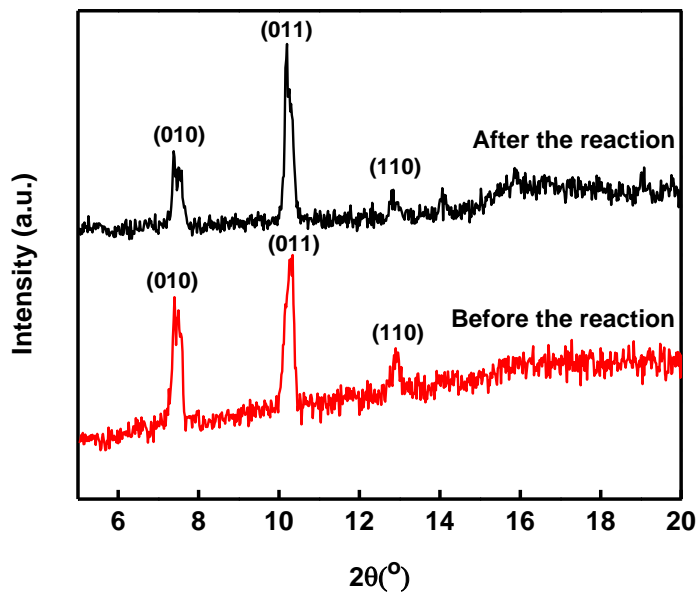


Fig. 19. XRD pattern of newly synthesized and recycled MIL-88-A

3.4.Solar/MIL-88-A/PS system

Experiments were done to study the effect of sunlight on NAP degradation. According to studies, NAP has been found to be photosensitive, where it shows a full degradation after a certain time from being exposed to sunlight [70–73]. In a 100 ml solution containing $[NAP]_0 = 50$ ppm, 25 mg L^{-1} of $[MIL-88-A]_0$ was added and left stirring in dark for a period of 1 hour to reach equilibrium adsorption, then the medium is spiked with $[PS] = 2$ mM, where continuous stirring was maintained to ensure uniform mixing and moved to be in sunlight. 1.5 mL samples were collected 30 seconds before and after the addition of MIL-88-A as well as before the addition of PS and every 5 mins for the next 25 mins then every 10 mins till 125 mins, where the reaction time was set to be around 2 hours. All controls show

full degradation after 30 mins after being exposed to sunlight, showing that NAP is photosensitive and can be degraded alone in sunlight (Fig. 20). The result obtained in the combined Solar/MIL-88-A/PS system (Fig. 20) has an added advantage to degrading NAP alone, where the degradation of its by-products was clearly noticed (Fig. 21).

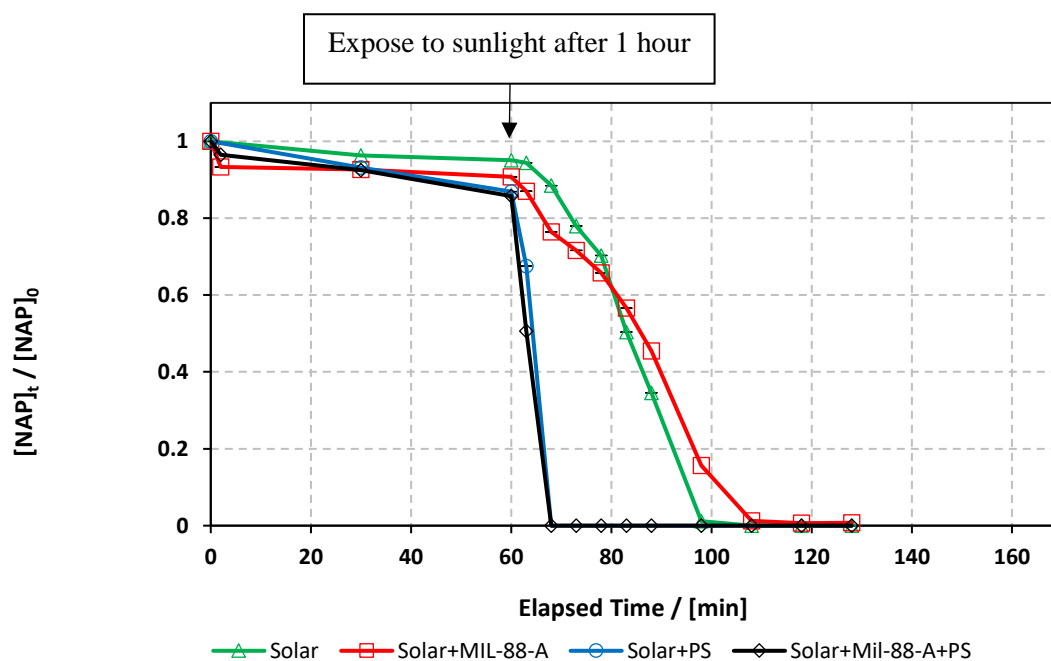


Fig. 20. The % degradation of NAP irradiated with solar energy as function of time (min) under different conditions: PS only, MIL-88-A only, and MIL-88-A with PS. Reactors were put under sunlight in a rotisserie shaker. Experimental conditions: $[NAP]_0 = 50 \text{ mg L}^{-1}$, $[PS]_0 = 2 \text{ mM}$, $[MIL-88-A]_0 = 25 \text{ mg L}^{-1}$. Error bars are calculated as $\frac{ts}{\sqrt{n}}$, where absent bars fall within the symbols.

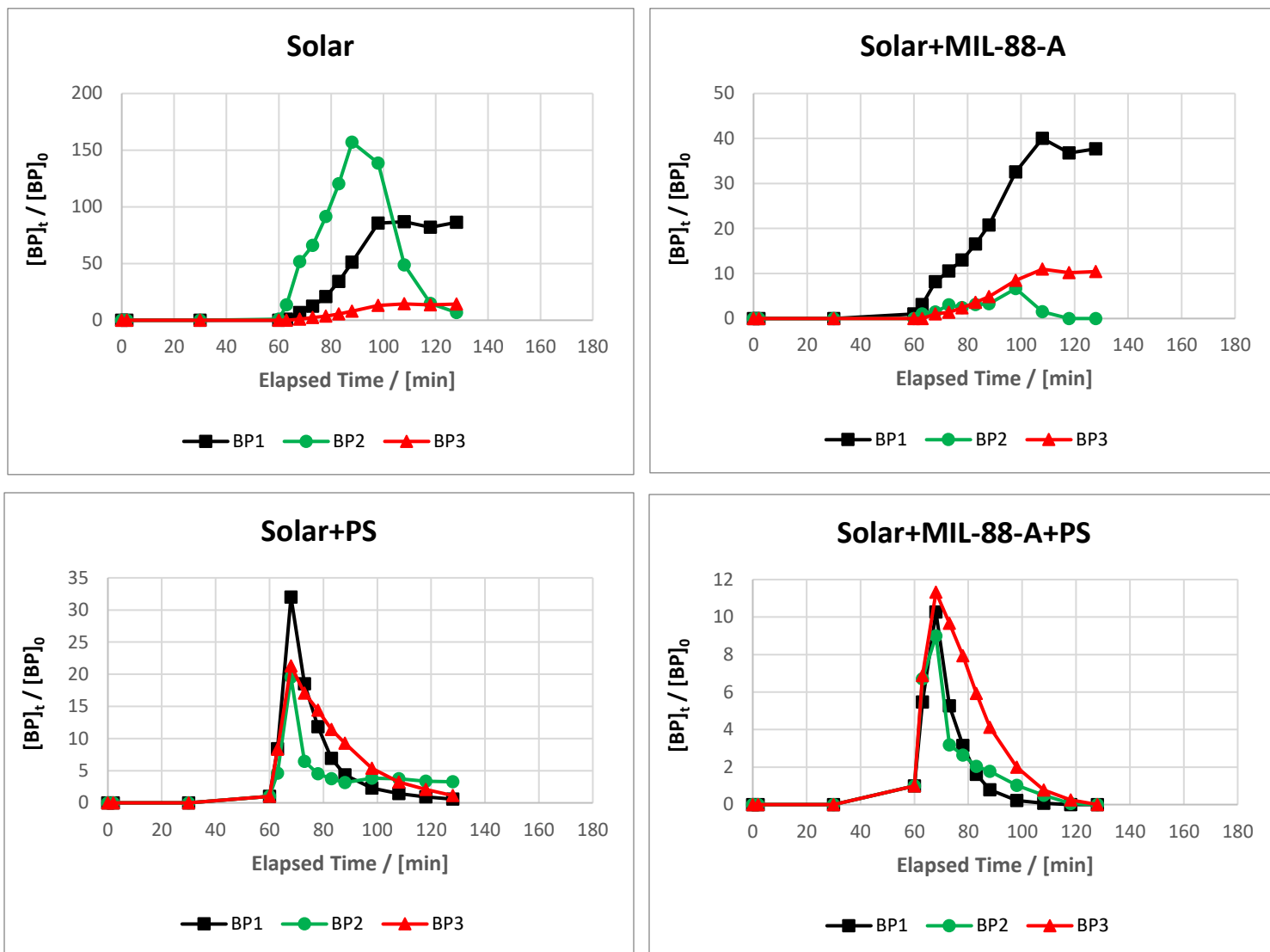


Fig. 21. Graphs showing the degradation of the by-products in Solar/MIL-88-A/PS system controls in the presence and/or absence of MIL-88-A and PS. Experimental conditions: $[NAP]_0 = 50 \text{ mg L}^{-1}$, $[PS]_0 = 2 \text{ mM}$, $[MIL-88-A]_0 = 25 \text{ mg L}^{-1}$.

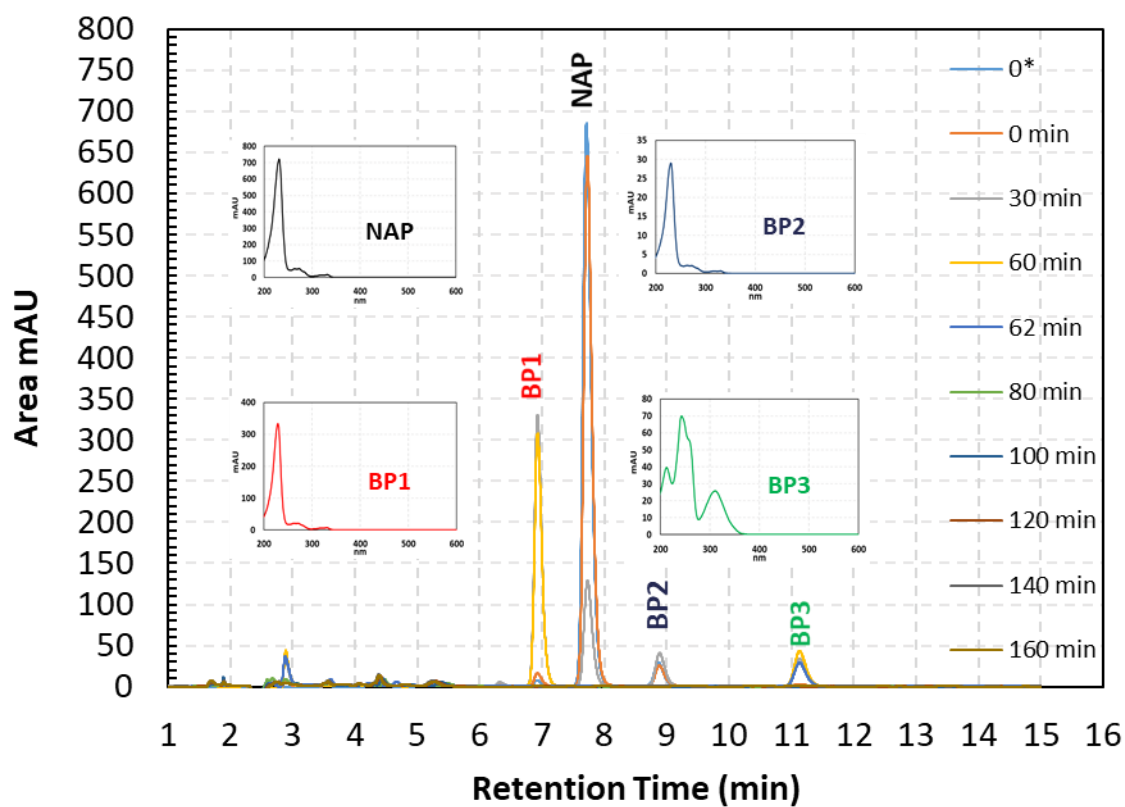


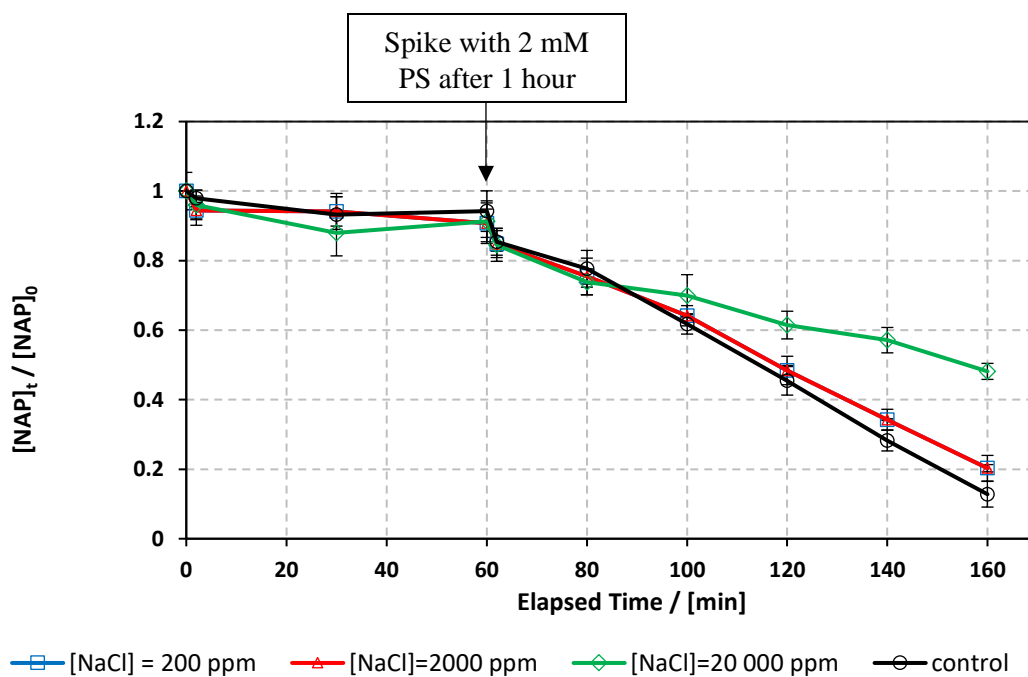
Fig. 22. Chromatogram of NAP extracted at 228 nm showing the by-products formed at 6.93, 8.73 and 11.13 min respectively under Solar/MIL-88-A/PS system.

3.5. Matrix effect

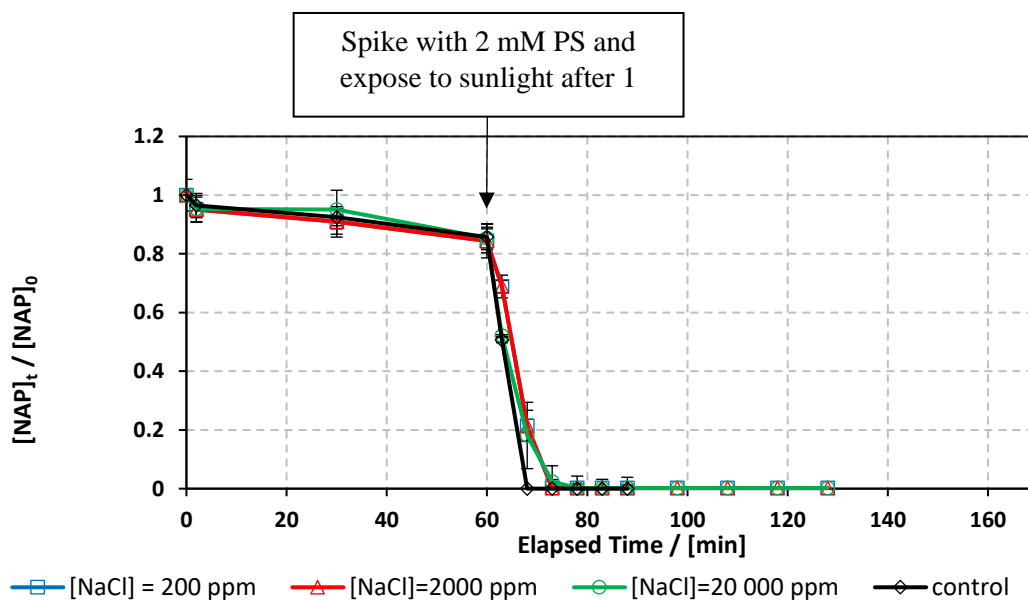
3.5.1. Case of chlorides

The effect of common anions in natural water was examined on NAP degradation in both UVA/MIL-88-A/PS/NAP and Solar/MIL-88-A/PS/NAP systems. To mimic natural water conditions, three different concentrations of chlorides corresponding to fresh water ($[\text{NaCl}] = 200 \text{ mg L}^{-1}$), brackish water ($[\text{NaCl}] = 2,000 \text{ mg L}^{-1}$), and saline water ($[\text{NaCl}] = 20,000 \text{ mg L}^{-1}$) were tested. The effect of chlorides in UVA/MIL-88-A/PS/NAP shows a slight inhibition in the % degradation of NAP in fresh and brackish water, while it shows a noticeable inhibition in saline water. This is due to the excess of Cl^- that would scavenge Cl^\bullet to produce dichloride radicals [74]. In Solar/MIL-88-A/PS/NAP system, the effect of chloride ions in the three different concentrations had no significant effect on NAP degradation, but they had on the degradation products (Fig. 24), where in free NaCl system under solar radiation, NAP and its degradation products undergoes a full degradation





(a)



(b)

Fig. 23 Effect of $[\text{NaCl}] = 200 - 20,000 \text{ mg L}^{-1}$ on the degradation of NAP as function of time (min): (a) in the UVA/MIL-88-A/PS/NAP system and (b) in the solar/MIL-88-A/PS/NAP system. Experimental conditions $[\text{NAP}]_0 = 50 \text{ ppm}$, $[\text{PS}]_0 = 2 \text{ mM}$, $[\text{MIL-88-A}]_0 = 25 \text{ mg L}^{-1}$. Error bars are calculated as $\frac{ts}{\sqrt{n}}$ where absent bars fall within the symbols.

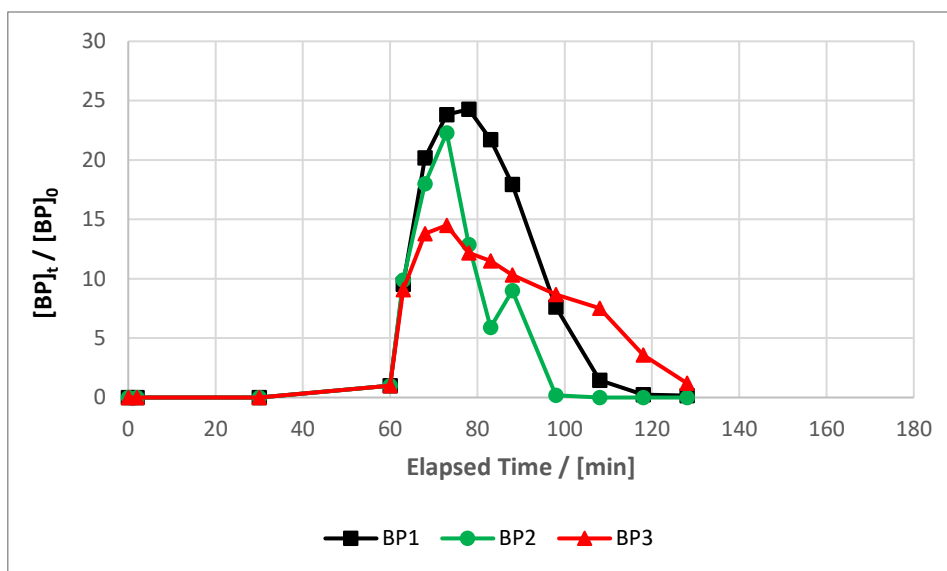


Fig. 24. Degradation by-products of NAP under chloride effect in Solar/MIL-88-A/PS. Experimental conditions $[NAP]_0 = 50$ ppm, $[PS]_0 = 2$ mM, $[MIL-88-A]_0 = 25$ mg L⁻¹, $[NaCl] = 20,000$ mg L⁻¹.

3.5.2. Case of carbonates

Bicarbonate effect was also examined in both UVA/MIL-88-A/PS/NAP and Solar/MIL-88-A/PS/NAP systems. Bicarbonate presence in the UVA/MIL-88-A/PS/NAP system shows a noticeable inhibition in the degradation of NAP. The drop of $[NAP]$ at $[NaHCO_3] = 1, 50$ and 100 mM after spiking with PS decreased from 87.2% to 28.5%, 21.5% and 33.3% respectively. However, in the Solar/MIL-88-A/PS/NAP system, there was a full degradation of NAP but not the by-products as in the bicarbonate free system (Fig. 26). $NaHCO_3$ inhibitory effect can be due to the reaction between HCO_3^- and sulfate radicals (SRs) yielding $CO_3^{\bullet-}$ ($E^\circ = 1.59$ V) which has moderate oxidative properties compared to sulfate radicals towards NAP. An increase in the pH of the reactive medium was noticed. The pH of the

solution increased with increasing HCO_3^- . This plays a major role in the inhibitory effect on the degradation of NAP.

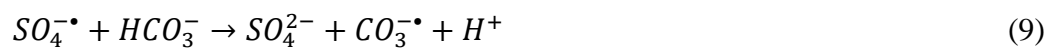
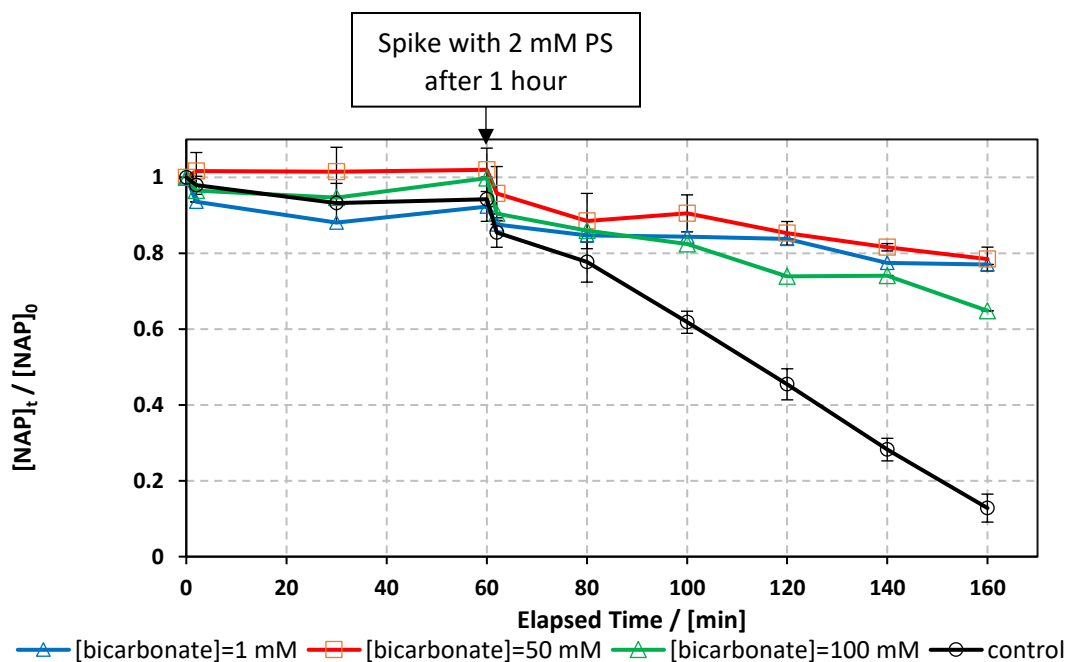
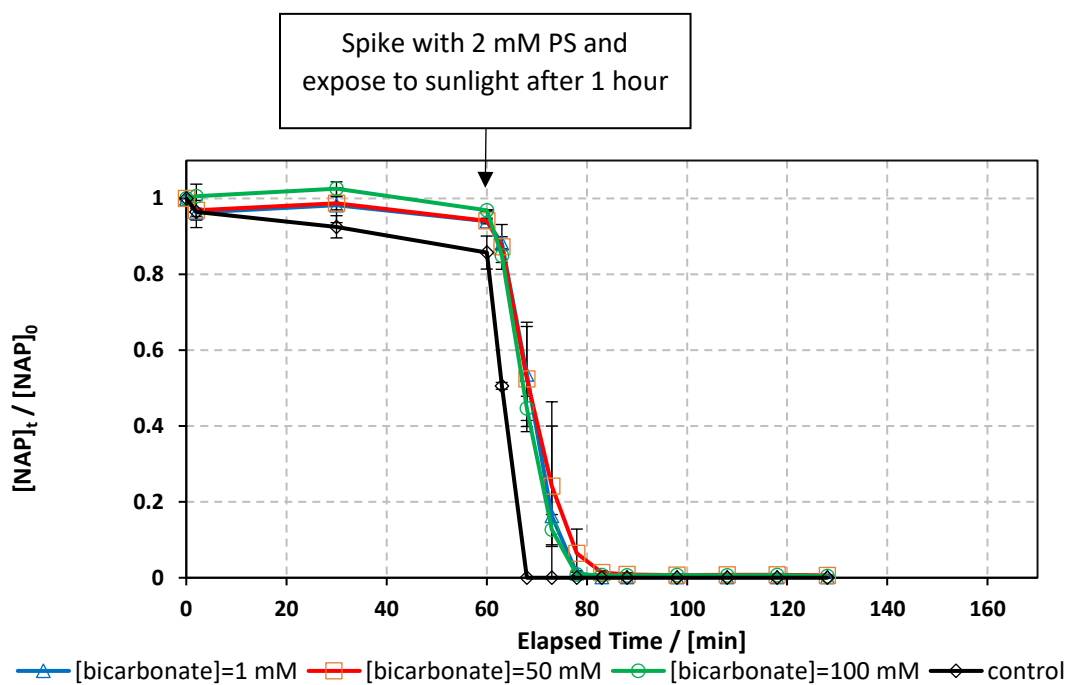


Table 1. (a) pH values of the different reaction system during the experiment in the UVA/MIL-88-A/PS/NAP system and (b) pH values of the different reaction system during the experiment in the Solar/MIL-88-A/PS/NAP system

	pH initial	pH final
$[\text{HCO}_3^-]$ free	6.10	3.73
$[\text{HCO}_3^-] = 1 \text{ mM}$	8.05	7.02
$[\text{HCO}_3^-] = 50 \text{ mM}$	8.59	8.54
$[\text{HCO}_3^-] = 100 \text{ mM}$	8.56	8.59
(a)		
	pH initial	pH final
$[\text{HCO}_3^-]$ free	6.12	2.51
$[\text{HCO}_3^-] = 1 \text{ mM}$	8.09	2.88
$[\text{HCO}_3^-] = 50 \text{ mM}$	9.04	8.78
$[\text{HCO}_3^-] = 100 \text{ mM}$	8.84	8.91
(b)		



(a)



(b)

Fig. 25. Effect of different carbonate concentration $[\text{CO}_3^{2-}] = 1 - 100 \text{ mM}$ on the degradation of NAP as function of time (min): (a) in the UVA/ MIL-88-A/PS/NAP system and (b) in the solar/MIL-88-A/PS/NAP system. Experimental conditions $[\text{NAP}]_0 = 50 \text{ ppm}$, $[\text{PS}]_0 = 2 \text{ mM}$, $[\text{MIL-88-A}]_0 = 25 \text{ mg L}^{-1}$. Error bars are calculated as $\frac{ts}{\sqrt{n}}$ where absent bars fall within the symbols.

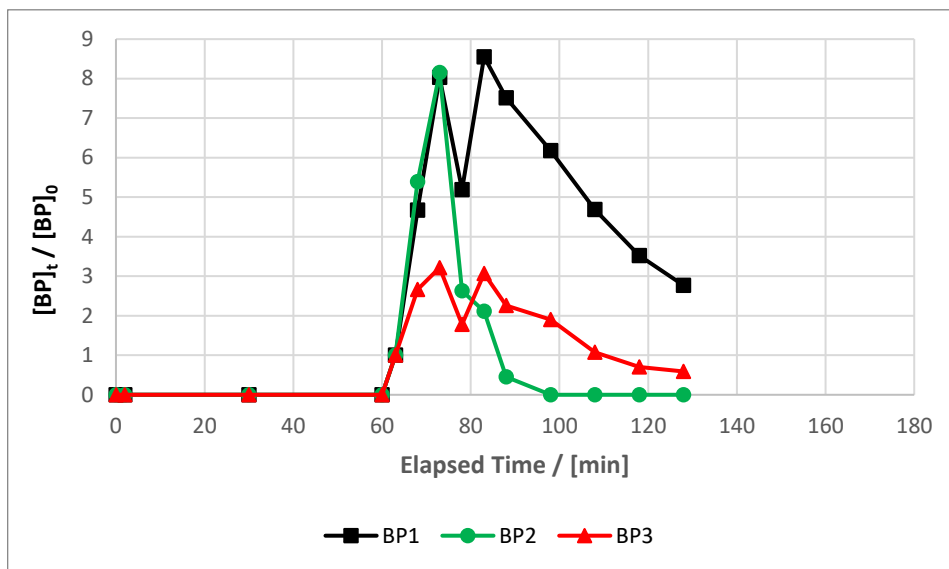
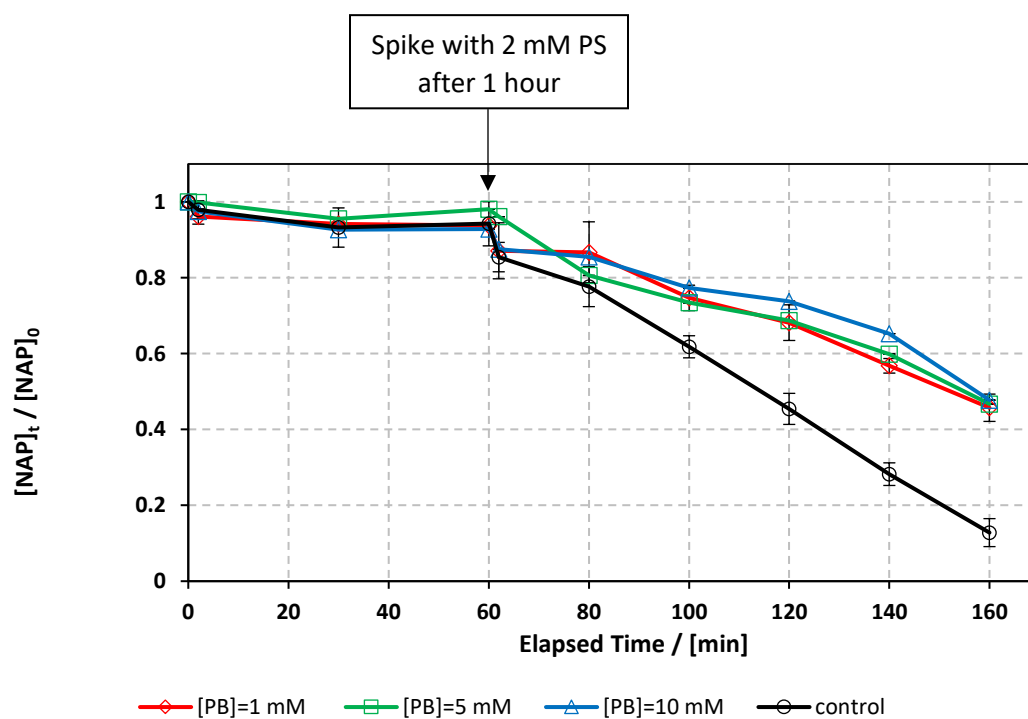


Fig. 26. Degradation by-products of NAP under carbonate effect in Solar/MIL-88-A/PS. Experimental conditions $[NAP]_0 = 50$ ppm, $[PS]_0 = 2$ mM, $[MIL-88-A]_0 = 25$ mg L⁻¹, $[CO_3^{2-}] = 100$ mM.

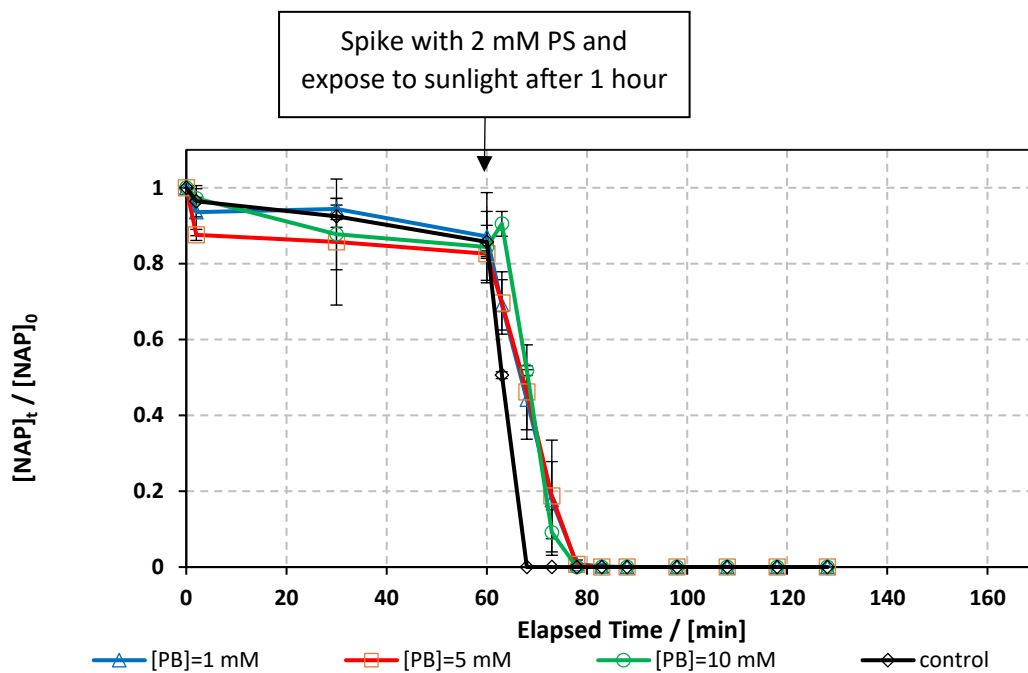
3.5.3. Case of phosphate

The effect of phosphate concentration on the degradation of NAP was investigated in both UVA/MIL-88-A/PS/NAP and Solar/MIL-88-A/PS/NAP systems for two reasons. First, to account for phosphate residues that may elude from conventional wastewater treatment methods [75]. Second, to study the effect of pH on the degradation of NAP. Thus, a study on the effect of phosphate buffer (PB) was conducted at three different concentrations 1, 5 and 10 mM of PB (pH = 4). Results shows that PB has an inhibitory effect on the degradation process of NAP in both systems. The degradation rate decreased to around 50% in UVA/MIL-88-A/PS/NAP system. However, in the Solar/MIL-88-A/PS/NAP system, there was a full degradation of NAP but not the by-products as in the phosphate free system (Fig. 28). This can be explained by the fact that phosphate species form stable complexes with

Fe^{2+} ions and accumulate on the surface of MIL-88-A, Thus, free Fe^{2+} ions in solution or adsorbed on the surface of the MOF prevent the chemical activation of PS. It was demonstrated in two independent studies on the degradation of sulfamethoxazole (SMX) and ranitidine in Fe/PS systems [26,76].



(a)



(b)

Fig. 27. Effect of different phosphate concentration $[\text{PO}_4^{3-}] = 1 - 10 \text{ mM}$ on the degradation of NAP as function of time (min): (a) in the UVA/ MIL-88-A/PS/NAP system and (b) in the Solar/MIL-88-A/PS/NAP system. Experimental conditions $[\text{NAP}]_0 = 50 \text{ ppm}$, $[\text{PS}]_0 = 2 \text{ mM}$, $[\text{MIL-88-A}]_0 = 25 \text{ mg L}^{-1}$. Error bars are calculated as $\frac{ts}{\sqrt{n}}$ where absent bars fall within the symbols.

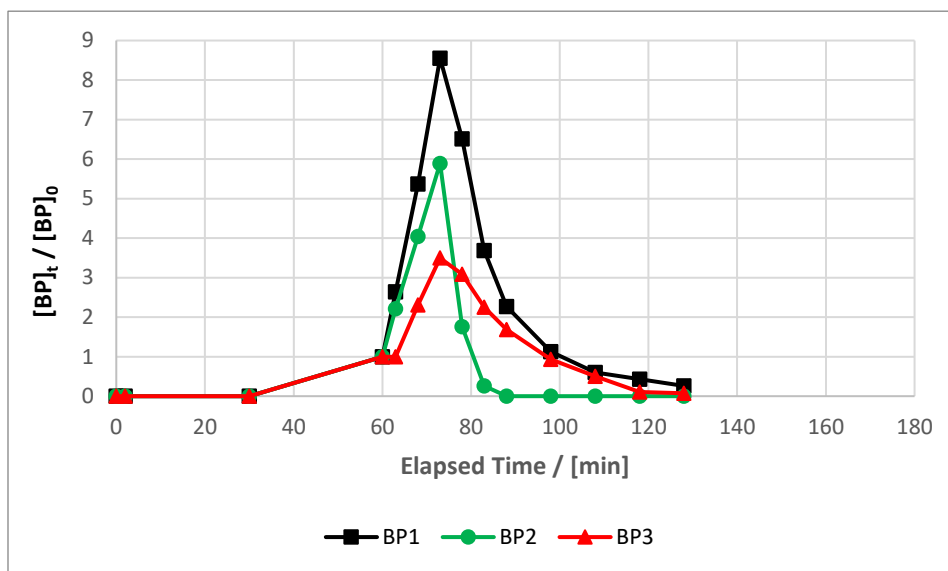
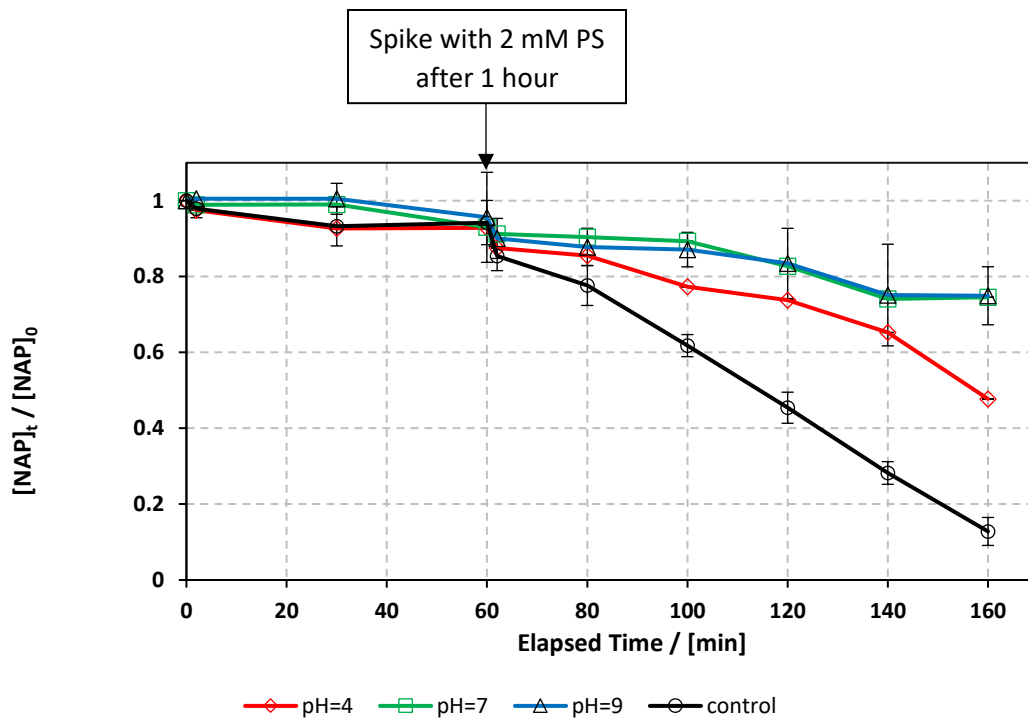


Fig. 28. Degradation by-products of NAP under phosphate effect in Solar/MIL-88-A/PS. Experimental conditions $[NAP]_0 = 50$ ppm, $[PS]_0 = 2$ mM, $[MIL-88-A]_0 = 25$ mg L⁻¹, $[PO_4^{3-}] = 10$ mM.

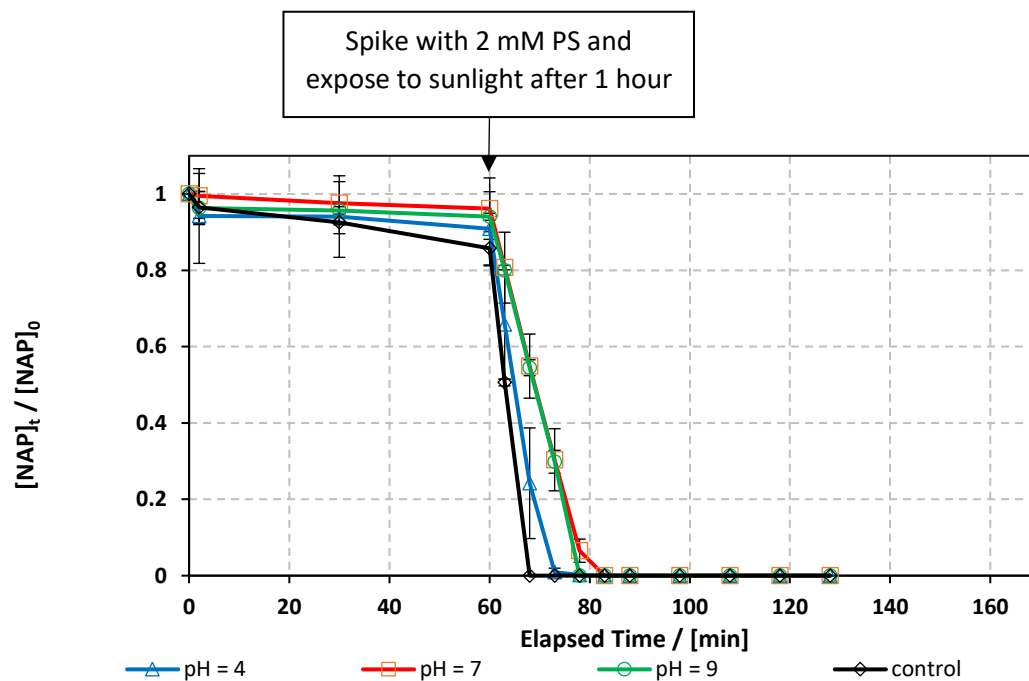
3.5.4. pH effect

pH value of the system is a major factor that affects the degradation of NAP. The effect of pH on the degradation of NAP in UVA/MIL-88-A/PS/NAP and Solar/MIL-88-A/PS/NAP systems was studied in 10 mM PB solutions with different pH values mimicking acidic, basic, and neutral conditions. The results showed inhibitory effect in both systems. In UVA/MIL-88-A/PS/NAP system the degradation rate decreases to 50% in acidic conditions (pH = 4), and around 25% in neutral and basic conditions. However, in the Solar/MIL-88-A/PS/NAP system, there was a full degradation of NAP but not the by-products as in the control system. This may be due to the absorption of OH ions on the

catalyst's surface inhibits the generation of hydroxyl radicals, which are responsible for the degradation process; as a result, the degradation efficiency reduces.



(a)



(b)

Fig. 29. Effect of pH values on the degradation of NAP as function of time (min): (a) in the UVA/ MIL-88-A/PS/NAP system and (b) in the Solar/MIL-88-A/PS/NAP system. Experimental conditions $[NAP]_0 = 50$ ppm, $[PS]_0 = 2$ mM, $[MIL-88-A]_0 = 25$ mg L⁻¹. Error bars are calculated as $\frac{ts}{\sqrt{n}}$ where absent bars fall within the symbols.

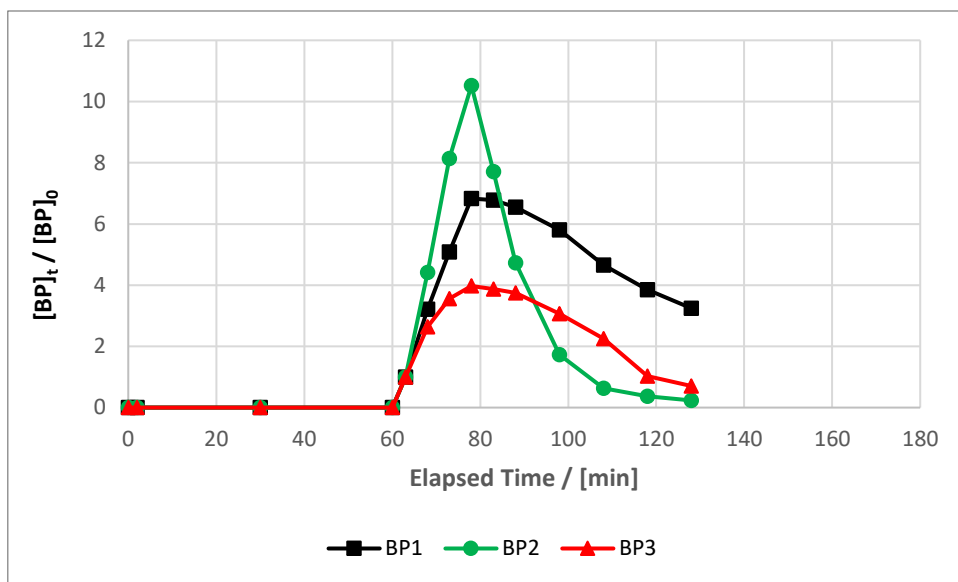


Fig. 30. Degradation by-products of NAP under pH effect in Solar/MIL-88-A/PS. Experimental conditions $[NAP]_0 = 50$ ppm, $[PS]_0 = 2$ mM, $[MIL-88-A]_0 = 25$ mg L⁻¹, pH = 9.

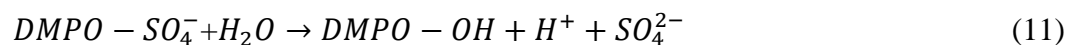
3.5.5. EPR measurements

Although AOP PS-based systems rely mainly on the formation of SRs and HRs upon activation, it is more likely that identification of these species via competitive kinetics using quenchers such as TBA and MeOH is not very accurate due to strong interferences between quenchers and the active sites of MIL-88-A, the heterogeneous catalysts. As a result, with the use of common 5,5-dimethyl-L-pyrroline N-oxide (DMPO) as the free radical trapping agent, the EPR technique was chosen as an appropriate analytical technique capable of identifying the presence of radicals and better understanding the role of the expected ROS in the catalytic system of MIL-88-A/PS [76–78].

In order to conduct a valid comparative analysis, EPR analysis was done on four different systems: System 1 (MIL-88-A), System 2 (PS), System 3 (MIL-88-A/PS) and

System 4 (MIL-88-A/PS/NAP). As it can be noticed from Fig. 32, non-significant peaks were present in System 1 compared to the peaks that are shown in the other three studied systems (2-4). To further understand the results of the EPR spectra acquired, a simulation using the Easyspin library for MATLAB and the rotational tumbling (5×10^{-11} s) and 'chili' functions was performed on the EPR spectra [79]. The results obtained showed the presence DMPO-OH adducts of intensity 1:2:2:1 and a hyperfine splitting constant of $a_N = a_H = 1.49$ mT. The second series was attributed to DMPO-CH₃ adducts, which showed a series of six peaks with an intensity of about 1:1:1:1:1:1 and a hyperfine splitting constant of $a_N = 1.58$ mT and $a_H = 2.58$ mT, respectively (Fig. 31). Alkyl leaching from the organic starting material, such as fumaric acid, with which MIL-88-A was synthesized, or ethanol impurity that remained adsorbed on the surface of MIL-88-A after washing could both contribute to the presence of methyl radical. As previously proven, the OH radicals present in System 1 can be produced by the photocatalytic activity of MIL-88-A in solution under day light [80]. System 2 demonstrated a better DMPO-OH adduct signal, with more defined peaks related to the net and clear formation of HRs. In fact, as the measurement time duration was increased to reduce background, PS was slightly activated at room temperature to create DMPO-SO₄⁻ adducts with very short lifetimes. A logical explanation would favor the formation of DMPO-OH adducts in aqueous medium, either through direct trapping of the generated HRs (Eq. (10)) or through nucleophilic substitution of the DMPO-SO₄⁻ (Eq. (11)), as previously observed [81]. When both PS and MIL-88-A are in present solution (upper curve, System 4), the DMPO-OH signal is significantly improved, as seen by its high intensity when compared to the MIL-88-A-free system (System 2). This could be owing to the above-mentioned rapid

conversion of SRs to HRs. Simultaneously, the existence of DMPO-CH₃ adduct in System 4 can be detected as in the absence of PS (System 1). The EPR spectra of System 3 also confirmed radical consumption in the reactive medium. In fact, the strength of the DMPO-OH adduct reduced because NAP in the medium consumes a large number of HRs and, indirectly SRs. This shows that some catalytically generated radicals, such as SRs and HRs, reacted with the NAP probe rather than the DMPO, resulting in less trapping. Because of its short lifespan and instability in solution, the DMPO-SO₄ adduct was not detected. Finally, EPR data indicated the presence of HRs and SRs in solution, as well as their coexistence, at least at the start of the oxidation reaction. As a result, it is possible to deduce that NAP degradation occurs via radical reaction in the reactive medium.



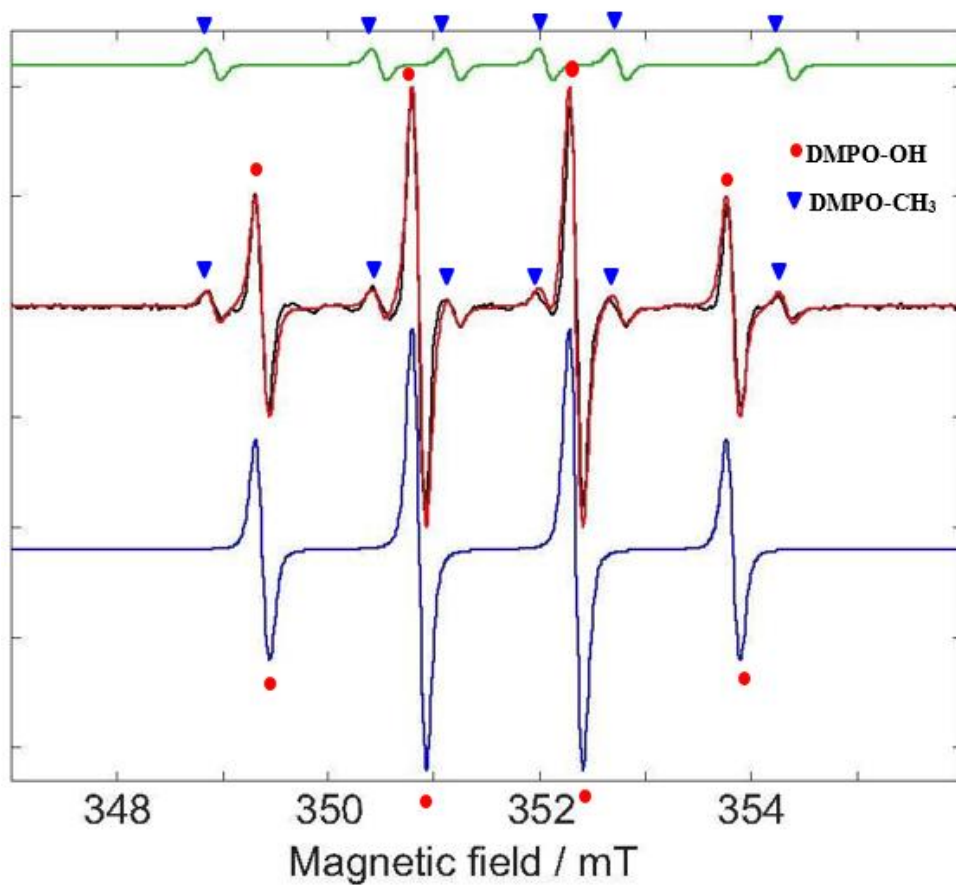


Fig. 31 EPR spectra. Green – simulated EPR spectrum for trapped methyl radicals. $a_N = 1.58$ mT, $a_H = 2.28$ mT. Blue – simulated EPR spectrum for trapped hydroxyl radicals. $a_N = 1.49$ mT, $a_H = 1.49$ mT. Red – the sum of the above two simulated trapped radical spectra. Black – experimental EPR spectrum under the following Experimental conditions: [PS] = 2.5 mM, [MIL-88-A] = 12.5 mg L⁻¹, [DMPO] = 100 mM.

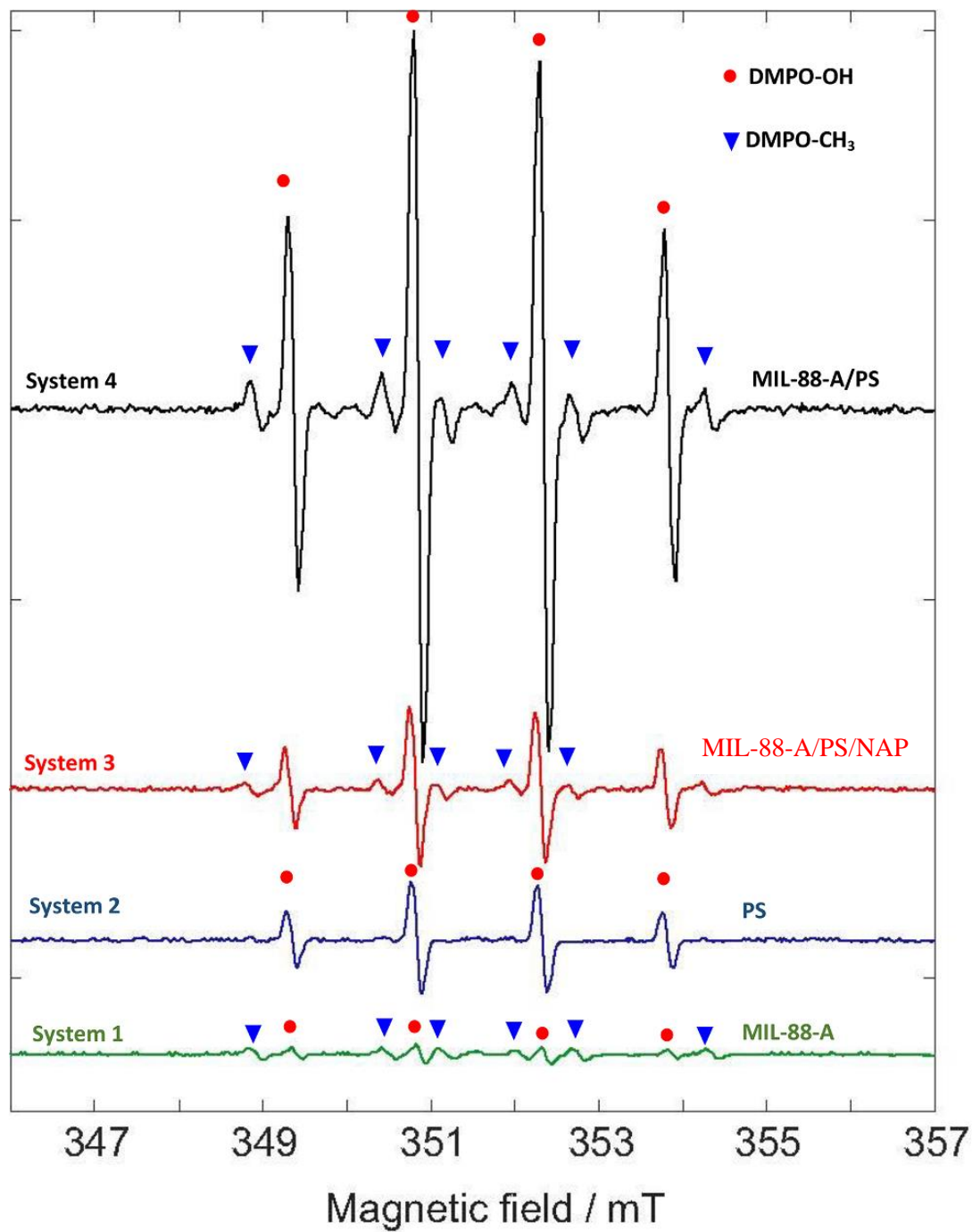


Fig. 32 . EPR spectra of DMPO-radical adducts in different reaction systems. Experimental conditions: [PS] = 2.5 mM, [MIL-88-A] = 12.5 mg L⁻¹, [DMPO] = 100 mM. The acquisition duration of EPR spectra is about 100 min for all systems.

3.5.6. Degradation mechanism

3.5.6.1 Identification of degradation products

As shown in Fig. 33, NAP indicated the presence of three byproducts when degraded in a MOF-activated PS system under the current experimental conditions. The identity of these byproducts is further investigated using high-resolution mass spectrometry.

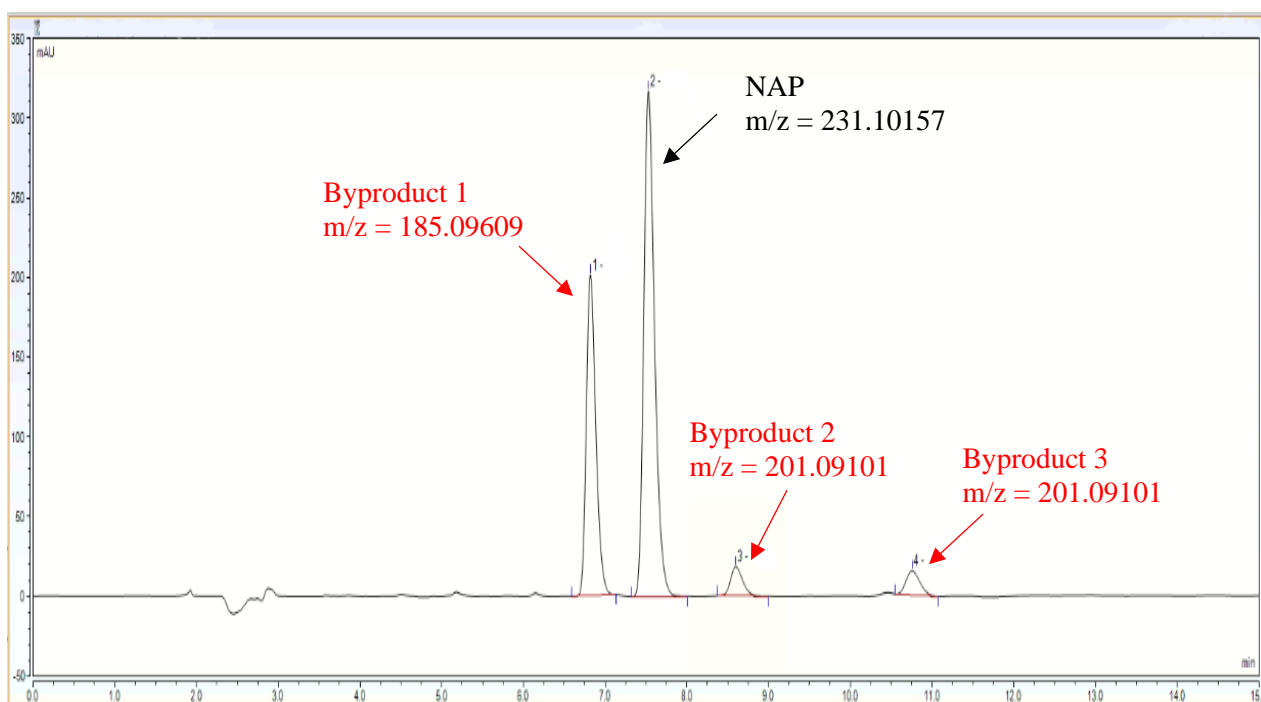


Fig. 33. HPLC chromatogram at $T = 25\text{ }^{\circ}\text{C}$ showing NAP and its byproducts at reaction time $t = 100$ mins.

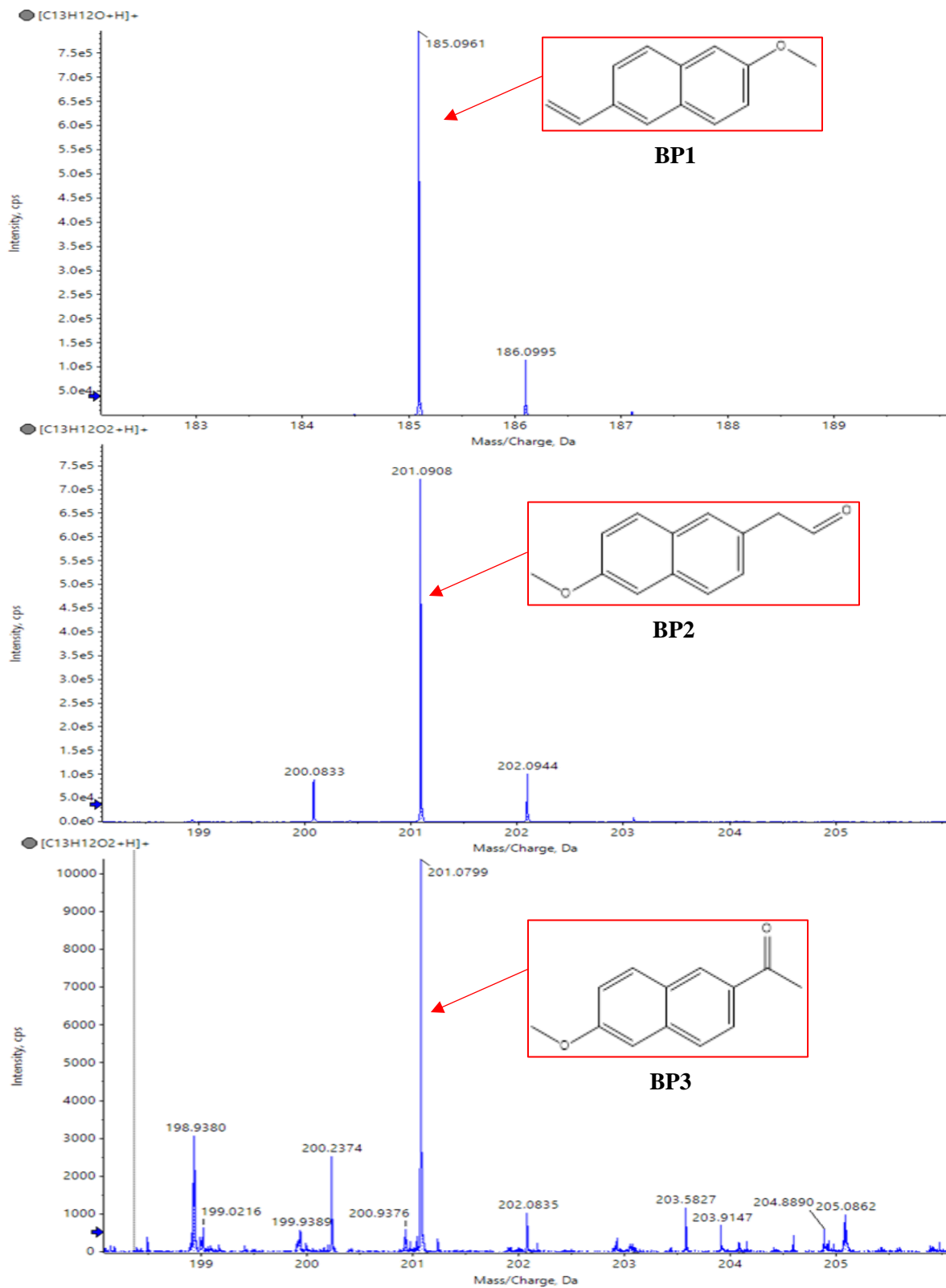


Fig. 34. Mass spectrum fragmentation pattern of BP1, BP2 and BP3

3.5.6.2. Proposed mechanism Surface based activation of PS on MIL-88-A

According to the EPR measurements, the elimination of NAP in UVA/MIL-88-A/PS system was mainly due to a radical process. MIL-88-A contains trivalent Fe active species, which come from the ferric chloride salt used in the synthesis process, where PS chemical activation may occur via a one-electron reduction mechanism. (Eqs. (12) and (13)) as it was previously proven [68,80,82].



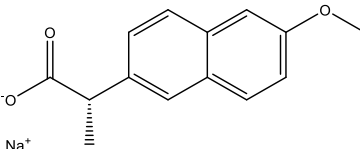
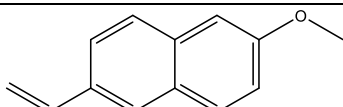
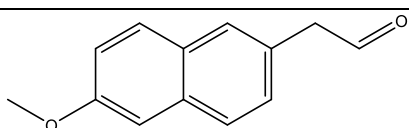
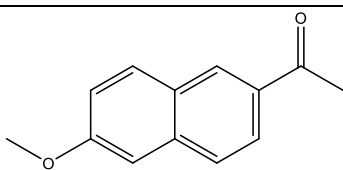
Fe^{2+} may be present due to Fe^{3+} reduction, producing persulfate radicals but in the presence of air or oxygen, it is quickly oxidized to Fe^{3+} , generating sulfate radicals that are responsible for degradation of NAP molecules.

3.5.6.2 Proposed NAP degradation mechanism

To have a better understanding of the NAP degradation mechanism, TOF-SIMS technique was used in addition to mass spectroscopy, SCIEX X500R QTOF, to detect and identify NAP degradation products in UVA/MIL-88-A/PS/NAP and Solar/MIL-88-A/PS/NAP systems. The TOF-SIMS technique enabled us to generate images of MIL-88-A based on specific atoms or molecular fragments extracted from the overall mass spectrum acquired by the software and from each pixel of the area of interest. The MIL-88-A fibers-like morphology of 3–8 μm length (Fig. 35a) and the distribution of NAP into the interstices of the fibers (Fig. 35b) are easily visible in the image of the total positive secondary ion collected. The green

color in Fig. 35b could be due to NAP by-products BP1 and BP2, as well as decarboxylated NAP at 185.1 m/z (Fig. 12b). The results clearly showed that adsorption and degradation are the two processes responsible for NAP elimination. Furthermore, SCIEX X500R QTOF, was used for accurate determination of the obtained by-products with the designed structure (error ≤ 2 ppm). Pathway I is the result of NAP decarboxylation caused by SRs attacking ET, whereas Pathway II is the result of a decarboxylation/dehydration mechanism occurring after hydroxylation triggered by HRs removing hydrogen from NAP. BP1 (m/z = 185.09609) is oxidized in the presence of HRs to form two intermediates, which are then further oxidized by HRs, generating BP2 and BP3 with the same molecular weight (m/z = 201.09101).

Table 2. NAP and byproducts identified by MS.

Compound	Molecular formula	ESI mode	<i>m/z</i>	R.T. (min)	Proposed structure
NAP	C ₁₄ H ₁₄ O ₃ ·Na ⁺	Positive	231.10157	7.50	
BP1	C ₁₃ H ₁₂ O	Positive	185.09609	6.30	
BP2	C ₁₃ H ₁₂ O ₂	Positive	201.09101	8.06	
BP3	C ₁₃ H ₁₂ O ₂	Positive	201.09101	9.97	

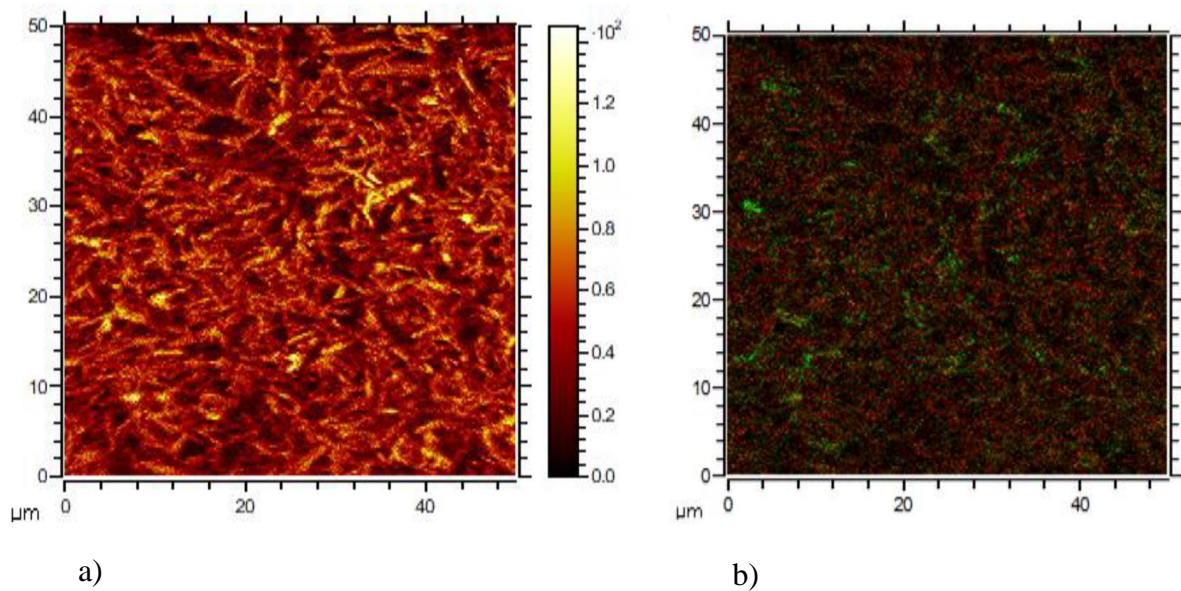


Fig. 35. (a) Image of the sum of all positives secondary ions of the MIL-88-A as prepared in the presence of NAP and PS at $t = 80$ min. The color scale goes from black (lack of emission) to white (saturated emission). (b) Overlay of the characteristic peak of MIL-88-A, Fe^+ ion at m/z 56 image (red color) and the characteristic peak of decarboxylated NAP at m/z 185.1 image (green color).

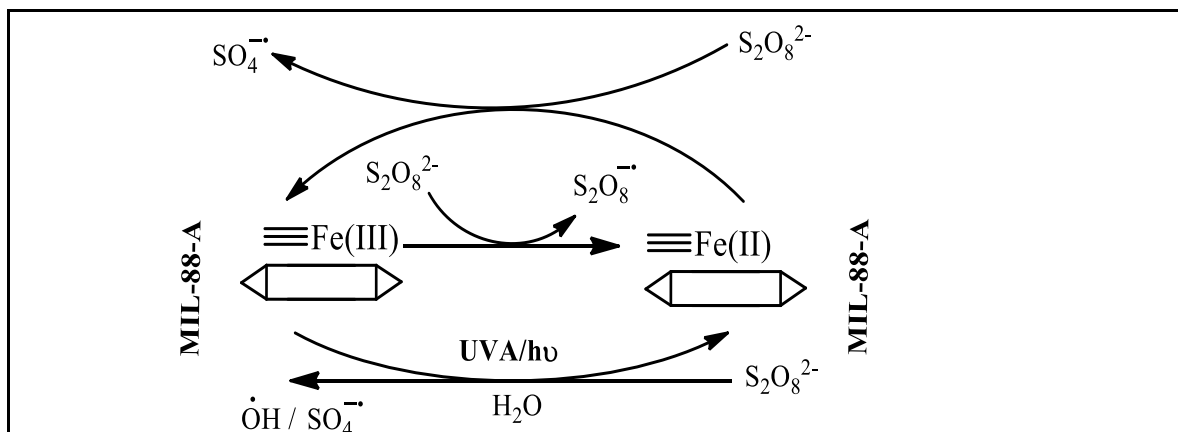


Fig. 36. Activation mechanism of PS in the UVA/MIL-88-A system

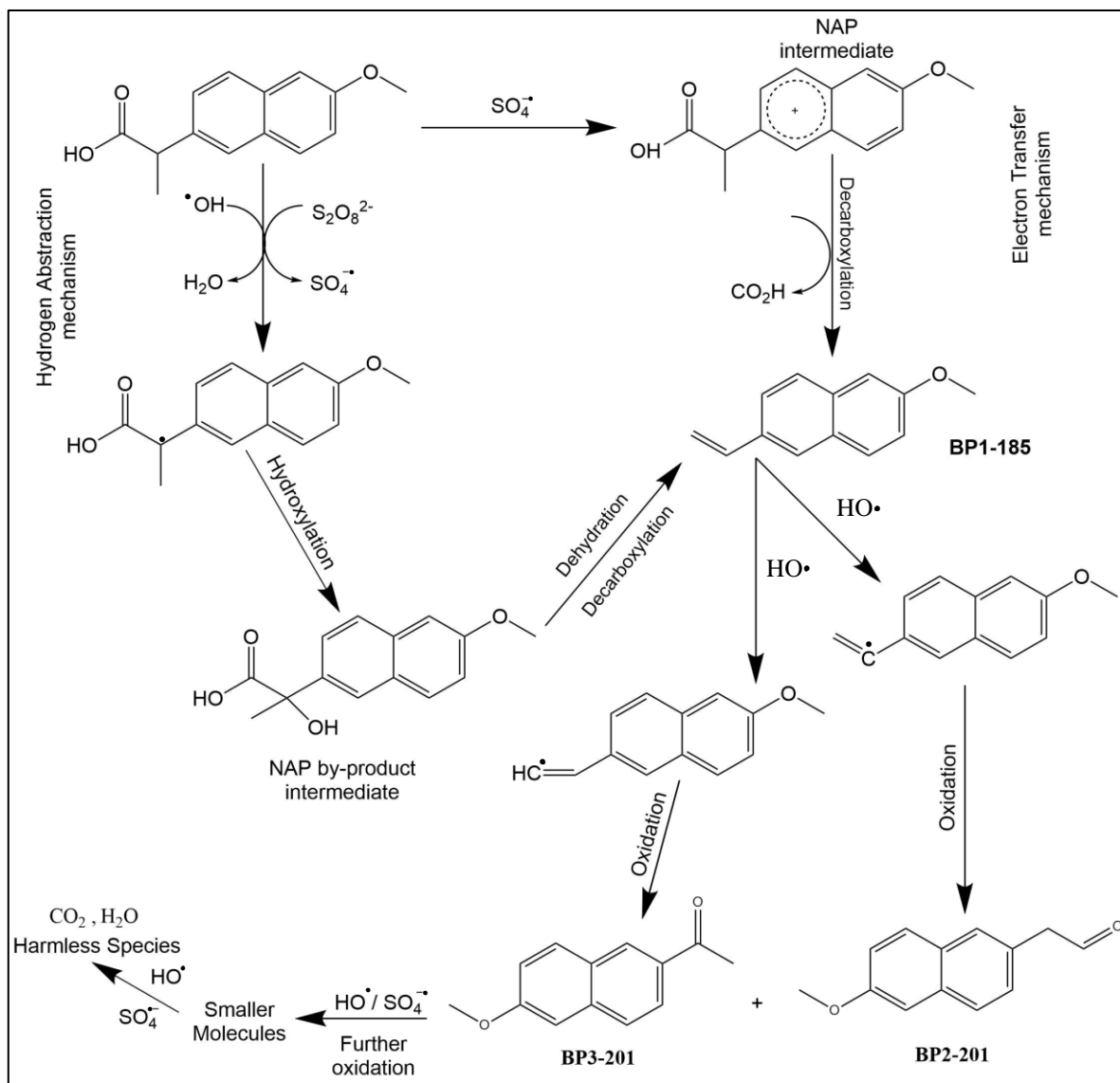


Fig. 37. Overall degradation mechanism of NAP in the UVA/MIL-88-A/PS system.

CHAPTER 4

CONCLUSION

In this study, pharmaceutical effluents, such as NAP, was efficiently degraded in PS-based AOPs system. MIL-88-A iron-based MOF catalyst synthesized in a green environment was to employed to improve previous findings. NAP degradation was compared using two different energy sources: UVA and Solar irradiation. Controls in the absence and presence of irradiation had no significant effect on the degradation of NAP. Both UVA and Solar were effective in a reasonable amount of time, where in Solar/MIL-88-A/PS system total degradation of NAP ($[NAP] = 50 \text{ ppm}$) was achieved in 10-15 minutes after spiking with PS. Results showed that MIL-88-A can be recycled and can be effective over three cycles in activation of PS without any regeneration process. MIL-88-A proved to be a potential heterogenous catalyst for PS activation in treatment of hazardous effluents in both UVA/MIL-88-A/PS and Solar/MIL-88-A/PS systems. Further research needed to be done is to investigate activation using concentrated solar power, and to modify MIL-88-A using additional functional groups to enhance catalytic efficiency or investigation of other activation techniques such as thermal, ultrasonic, and chemical.

REFERENCES

- [1] A.B.A. Boxall, M.A. Rudd, B.W. Brooks, D.J. Caldwell, K. Choi, S. Hickmann, E. Innes, K. Ostapyk, J.P. Staveley, T. Verslycke, G.T. Ankley, K.F. Beazley, S.E. Belanger, J.P. Berninger, P. Carriquiriborde, A. Coors, P.C. DeLeo, S.D. Dyer, J.F. Ericson, F. Gagné, J.P. Giesy, T. Gouin, L. Hallstrom, M. V. Karlsson, D.G. Joakim Larsson, J.M. Lazorchak, F. Mastrocco, A. McLaughlin, M.E. McMaster, R.D. Meyerhoff, R. Moore, J.L. Parrott, J.R. Snape, R. Murray-Smith, M.R. Servos, P.K. Sibley, J.O. Straub, N.D. Szabo, E. Topp, G.R. Tetreault, V.L. Trudeau, G. Van Der Kraak, Pharmaceuticals and personal care products in the environment: What are the big questions?, *Environ. Health Perspect.* 120 (2012) 1221–1229. <https://doi.org/10.1289/ehp.1104477>.
- [2] A.J. Ebele, M. Abou-Elwafa Abdallah, S. Harrad, Pharmaceuticals and personal care products (PPCPs) in the freshwater aquatic environment, *Emerg. Contam.* 3 (2017) 1–16. <https://doi.org/10.1016/j.emcon.2016.12.004>.
- [3] J.L. Liu, M.H. Wong, Pharmaceuticals and personal care products (PPCPs): A review on environmental contamination in China, *Environ. Int.* 59 (2013) 208–224. <https://doi.org/10.1016/j.envint.2013.06.012>.
- [4] J.L. Tambosi, L.Y. Yamanaka, H.J. José, R. De Fátima Peralta Muniz Moreira, H.F. Schröder, Recent research data on the removal of pharmaceuticals from sewage treatment plants (STP), *Quim. Nova.* 33 (2010) 411–420. <https://doi.org/10.1590/S0100-40422010000200032>.
- [5] P. Bottoni, S. Caroli, A.B. Caracciolo, Pharmaceuticals as priority water contaminants, *Toxicol. Environ. Chem.* 92 (2010) 549–565. <https://doi.org/10.1080/02772241003614320>.
- [6] K.E. Arnold, A.R. Brown, A.R. Brown, G.T. Ankley, J.P. Sumpter, Medicating the environment: Assessing risks of pharmaceuticals to wildlife and ecosystems, *Philos. Trans. R. Soc. B Biol. Sci.* 369 (2014). <https://doi.org/10.1098/rstb.2013.0569>.
- [7] V. Burkina, V. Zlabek, G. Zamaratskaia, Effects of pharmaceuticals present in aquatic environment on Phase I metabolism in fish, *Environ. Toxicol. Pharmacol.* 40 (2015) 430–444. <https://doi.org/10.1016/j.etap.2015.07.016>.
- [8] U. Memmert, A. Peither, R. Burri, K. Weber, T. Schmidt, J.P. Sumpter, A. Hartmann, Diclofenac: New data on chronic toxicity and bioconcentration in fish, *Environ. Toxicol. Chem.* 32 (2013) 442–452. <https://doi.org/10.1002/etc.2085>.
- [9] O. Cardoso, J.M. Porcher, W. Sanchez, Factory-discharged pharmaceuticals could be a relevant source of aquatic environment contamination: Review of evidence and

- need for knowledge, *Chemosphere*. 115 (2014) 20–30.
<https://doi.org/10.1016/j.chemosphere.2014.02.004>.
- [10] S. Zorita, L. Mårtensson, L. Mathiasson, Occurrence and removal of pharmaceuticals in a municipal sewage treatment system in the south of Sweden, *Sci. Total Environ.* 407 (2009) 2760–2770.
<https://doi.org/10.1016/J.SCITOTENV.2008.12.030>.
- [11] G.R. Boyd, J.M. Palmeri, S. Zhang, D.A. Grimm, Pharmaceuticals and personal care products (PPCPs) and endocrine disrupting chemicals (EDCs) in stormwater canals and Bayou St. John in New Orleans, Louisiana, USA, *Sci. Total Environ.* 333 (2004) 137–148. <https://doi.org/10.1016/J.SCITOTENV.2004.03.018>.
- [12] D. Ashton, M. Hilton, K. V. Thomas, Investigating the environmental transport of human pharmaceuticals to streams in the United Kingdom, *Sci. Total Environ.* 333 (2004) 167–184. <https://doi.org/10.1016/J.SCITOTENV.2004.04.062>.
- [13] N. Lindqvist, T. Tuhkanen, L. Kronberg, Occurrence of acidic pharmaceuticals in raw and treated sewages and in receiving waters, *Water Res.* 39 (2005) 2219–2228.
<https://doi.org/10.1016/J.WATRES.2005.04.003>.
- [14] N. Nakada, T. Tanishima, H. Shinohara, K. Kiri, H. Takada, Pharmaceutical chemicals and endocrine disrupters in municipal wastewater in Tokyo and their removal during activated sludge treatment, *Water Res.* 40 (2006) 3297–3303.
<https://doi.org/10.1016/J.WATRES.2006.06.039>.
- [15] M. Carballa, F. Omil, J.M. Lema, M. Llompart, C. García-Jares, I. Rodríguez, M. Gómez, T. Ternes, Behavior of pharmaceuticals, cosmetics and hormones in a sewage treatment plant, *Water Res.* 38 (2004) 2918–2926.
<https://doi.org/10.1016/J.WATRES.2004.03.029>.
- [16] T.A. Ternes, M. Meisenheimer, D. McDowell, F. Sacher, H.J. Brauch, B. Haist-Gulde, G. Preuss, U. Wilme, N. Zulei-Seibert, Removal of pharmaceuticals during drinking water treatment, *Environ. Sci. Technol.* 36 (2002) 3855–3863.
<https://doi.org/10.1021/es015757k>.
- [17] T. Heberer, Occurrence, fate, and removal of pharmaceutical residues in the aquatic environment: a review of recent research data, *Toxicol. Lett.* 131 (2002) 5–17.
[https://doi.org/10.1016/S0378-4274\(02\)00041-3](https://doi.org/10.1016/S0378-4274(02)00041-3).
- [18] R. Andreozzi, V. Caprio, A. Insola, R. Marotta, Advanced oxidation processes (AOP) for water purification and recovery, *Catal. Today.* 53 (1999) 51–59.
[https://doi.org/10.1016/S0920-5861\(99\)00102-9](https://doi.org/10.1016/S0920-5861(99)00102-9).
- [19] P.R. Gogate, A.B. Pandit, A review of imperative technologies for wastewater treatment I: Oxidation technologies at ambient conditions, *Adv. Environ. Res.* 8

- (2004) 501–551. [https://doi.org/10.1016/S1093-0191\(03\)00032-7](https://doi.org/10.1016/S1093-0191(03)00032-7).
- [20] S. YANG, P. WANG, X. YANG, G. WEI, W. ZHANG, L. SHAN, A novel advanced oxidation process to degrade organic pollutants in wastewater: Microwave-activated persulfate oxidation, *J. Environ. Sci.* 21 (2009) 1175–1180. [https://doi.org/10.1016/S1001-0742\(08\)62399-2](https://doi.org/10.1016/S1001-0742(08)62399-2).
- [21] C. Wei, F. Zhang, Y. Hu, C. Feng, H. Wu, Ozonation in water treatment: The generation, basic properties of ozone and its practical application, *Rev. Chem. Eng.* 33 (2017) 49–89. <https://doi.org/10.1515/REVCE-2016-0008/MACHINEREADABLECITATION/RIS>.
- [22] S.O. Ganiyu, M. Zhou, C.A. Martínez-Huitle, Heterogeneous electro-Fenton and photoelectro-Fenton processes: A critical review of fundamental principles and application for water/wastewater treatment, *Appl. Catal. B Environ.* 235 (2018) 103–129. <https://doi.org/10.1016/J.APCATB.2018.04.044>.
- [23] B.A. Wols, C.H.M. Hofman-Caris, Review of photochemical reaction constants of organic micropollutants required for UV advanced oxidation processes in water, *Water Res.* 46 (2012) 2815–2827. <https://doi.org/10.1016/J.WATRES.2012.03.036>.
- [24] J. Yan, L. Han, W. Gao, S. Xue, M. Chen, Biochar supported nanoscale zerovalent iron composite used as persulfate activator for removing trichloroethylene, *Bioresour. Technol.* 175 (2015) 269–274. <https://doi.org/10.1016/j.biortech.2014.10.103>.
- [25] N. Lindqvist, T. Tuhkanen, L. Kronberg, Occurrence of acidic pharmaceuticals in raw and treated sewages and in receiving waters, *Water Res.* 39 (2005) 2219–2228. <https://doi.org/10.1016/j.watres.2005.04.003>.
- [26] S. Naim, A. Ghauch, Ranitidine abatement in chemically activated persulfate systems: Assessment of industrial iron waste for sustainable applications, *Chem. Eng. J.* 288 (2016) 276–288. <https://doi.org/10.1016/j.cej.2015.11.101>.
- [27] A. Ghauch, G. Ayoub, S. Naim, Degradation of sulfamethoxazole by persulfate assisted micrometric Fe⁰ in aqueous solution, *Chem. Eng. J.* 228 (2013) 1168–1181. <https://doi.org/10.1016/j.cej.2013.05.045>.
- [28] M. Amasha, A. Baalbaki, S. Al Hakim, R. El Asmar, Degradation of a Toxic Molecule o-Toluidine in Industrial Effluents using UV254 / PS System Degradation of toxic molecules using persulfate as an oxidant View project Degradation of toxic molecules using persulfate as an oxidant View project, *Artic. J. Adv. Oxid. Technol.* (2018). <https://doi.org/10.26802/jaots.2017.0099>.
- [29] Y. Liu, X. He, Y. Fu, D.D. Dionysiou, Kinetics and mechanism investigation on the destruction of oxytetracycline by UV-254 nm activation of persulfate, *J. Hazard.*

- Mater. 305 (2016) 229–239. <https://doi.org/10.1016/J.JHAZMAT.2015.11.043>.
- [30] A. Ghauch, A. Baalbaki, M. Amasha, R. El Asmar, O. Tantawi, Contribution of persulfate in UV-254 nm activated systems for complete degradation of chloramphenicol antibiotic in water, *Chem. Eng. J.* 317 (2017) 1012–1025. <https://doi.org/10.1016/j.cej.2017.02.133>.
- [31] M. Amasha, A. Baalbaki, A. Ghauch, A comparative study of the common persulfate activation techniques for the complete degradation of an NSAID: The case of ketoprofen, *Chem. Eng. J.* 350 (2018) 395–410. <https://doi.org/10.1016/j.cej.2018.05.118>.
- [32] A. Ghauch, A.M. Tuqan, N. Kibbi, Ibuprofen removal by heated persulfate in aqueous solution: A kinetics study, *Chem. Eng. J.* 197 (2012) 483–492. <https://doi.org/10.1016/j.cej.2012.05.051>.
- [33] A. Ghauch, A.M. Tuqan, N. Kibbi, S. Geryes, Methylene blue discoloration by heated persulfate in aqueous solution, *Chem. Eng. J.* 213 (2012) 259–271. <https://doi.org/10.1016/J.CEJ.2012.09.122>.
- [34] M.G. Antoniou, A.A. de la Cruz, D.D. Dionysiou, Degradation of microcystin-LR using sulfate radicals generated through photolysis, thermolysis and e- transfer mechanisms, *Appl. Catal. B Environ.* 96 (2010) 290–298. <https://doi.org/10.1016/j.apcatb.2010.02.013>.
- [35] K.Y. Andrew Lin, H.A. Chang, C.J. Hsu, Iron-based metal organic framework, MIL-88A, as a heterogeneous persulfate catalyst for decolorization of Rhodamine B in water, *RSC Adv.* 5 (2015) 32520–32530. <https://doi.org/10.1039/c5ra01447f>.
- [36] N.A. Khan, Z. Hasan, S.H. Jung, Adsorptive removal of hazardous materials using metal-organic frameworks (MOFs): A review, *J. Hazard. Mater.* 244–245 (2013) 444–456. <https://doi.org/10.1016/j.jhazmat.2012.11.011>.
- [37] G. Férey, Hybrid porous solids: Past, present, future, *Chem. Soc. Rev.* 37 (2008) 191–214. <https://doi.org/10.1039/b618320b>.
- [38] P.Z. Moghadam, A. Li, S.B. Wiggin, A. Tao, A.G.P. Maloney, P.A. Wood, S.C. Ward, D. Fairen-Jimenez, Development of a Cambridge Structural Database Subset: A Collection of Metal-Organic Frameworks for Past, Present, and Future, *Chem. Mater.* 29 (2017) 2618–2625. <https://doi.org/10.1021/acs.chemmater.7b00441>.
- [39] J. Wang, J. Wan, Y. Ma, Y. Wang, M. Pu, Z. Guan, Metal-organic frameworks MIL-88A with suitable synthesis conditions and optimal dosage for effective catalytic degradation of Orange G through persulfate activation, *RSC Adv.* 6 (2016) 112502–112511. <https://doi.org/10.1039/C6RA24429G>.

- [40] P. Horcajada, R. Gref, T. Baati, P.K. Allan, G. Maurin, P. Couvreur, G. Férey, R.E. Morris, C. Serre, Metal-organic frameworks in biomedicine, *Chem. Rev.* (2012). <https://doi.org/10.1021/cr200256v>.
- [41] A.C. McKinlay, R.E. Morris, P. Horcajada, G. Férey, R. Gref, P. Couvreur, C. Serre, BioMOFs: Metal-organic frameworks for biological and medical applications, *Angew. Chemie - Int. Ed.* 49 (2010) 6260–6266. <https://doi.org/10.1002/anie.201000048>.
- [42] M. Kurmoo, Magnetic metal-organic frameworks, *Chem. Soc. Rev.* (2009). <https://doi.org/10.1039/b804757j>.
- [43] T. Uemura, N. Yanai, S. Kitagawa, Polymerization reactions in porous coordination polymers, *Chem. Soc. Rev.* (2009). <https://doi.org/10.1039/b802583p>.
- [44] J. Lee, O.K. Farha, J. Roberts, K.A. Scheidt, S.T. Nguyen, J.T. Hupp, Metal-organic framework materials as catalysts, *Chem. Soc. Rev.* (2009). <https://doi.org/10.1039/b807080f>.
- [45] S. Bhattacharjee, J.S. Choi, S.T. Yang, S.B. Choi, J. Kim, W.S. Ann, Solvothermal synthesis of Fe-MOF-74 and its catalytic properties in phenol hydroxylation, *J. Nanosci. Nanotechnol.* 10 (2010) 135–141. <https://doi.org/10.1166/jnn.2010.1493>.
- [46] J.J. Du, Y.P. Yuan, J.X. Sun, F.M. Peng, X. Jiang, L.G. Qiu, A.J. Xie, Y.H. Shen, J.F. Zhu, New photocatalysts based on MIL-53 metal-organic frameworks for the decolorization of methylene blue dye, *J. Hazard. Mater.* 190 (2011) 945–951. <https://doi.org/10.1016/j.jhazmat.2011.04.029>.
- [47] H. Liu, X. Ren, L. Chen, Synthesis and characterization of magnetic metal-organic framework for the adsorptive removal of Rhodamine B from aqueous solution, *J. Ind. Eng. Chem.* 34 (2016) 278–285. <https://doi.org/10.1016/j.jiec.2015.11.020>.
- [48] X. Li, W. Guo, Z. Liu, R. Wang, H. Liu, Fe-based MOFs for efficient adsorption and degradation of acid orange 7 in aqueous solution via persulfate activation, *Appl. Surf. Sci.* 369 (2016) 130–136. <https://doi.org/10.1016/j.apsusc.2016.02.037>.
- [49] E. Haque, J.E. Lee, I.T. Jang, Y.K. Hwang, J.S. Chang, J. Jegal, S.H. Jung, Adsorptive removal of methyl orange from aqueous solution with metal-organic frameworks, porous chromium-benzenedicarboxylates, *J. Hazard. Mater.* 181 (2010) 535–542. <https://doi.org/10.1016/J.JHAZMAT.2010.05.047>.
- [50] E.Y. Park, Z. Hasan, N.A. Khan, S.H. Jung, Adsorptive removal of bisphenol-a from water with a metal-organic framework, a porous chromium-benzenedicarboxylate, *J. Nanosci. Nanotechnol.* 13 (2013) 2789–2794. <https://doi.org/10.1166/JNN.2013.7411>.

- [51] S. Yuan, L. Feng, K. Wang, J. Pang, M. Bosch, C. Lollar, Y. Sun, J. Qin, X. Yang, P. Zhang, Q. Wang, L. Zou, Y. Zhang, L. Zhang, Y. Fang, J. Li, H.C. Zhou, Stable Metal–Organic Frameworks: Design, Synthesis, and Applications, *Adv. Mater.* 30 (2018). <https://doi.org/10.1002/ADMA.201704303>.
- [52] M. Tong, D. Liu, Q. Yang, S. Devautour-Vinot, G. Maurin, C. Zhong, Influence of framework metal ions on the dye capture behavior of MIL-100 (Fe, Cr) MOF type solids, *J. Mater. Chem. A*. 1 (2013) 8534–8537. <https://doi.org/10.1039/C3TA11807J>.
- [53] A.J. Paine, Mechanisms of chromium toxicity, carcinogenicity and allergenicity: Review of the literature from 1985 to 2000, *Hum. Exp. Toxicol.* 20 (2001) 439–451. <https://doi.org/10.1191/096032701682693062>.
- [54] M. Özcan, A. Allahbeickaraghi, M. Dündar, Possible hazardous effects of hydrofluoric acid and recommendations for treatment approach: A review, *Clin. Oral Investig.* 16 (2012) 15–23. <https://doi.org/10.1007/S00784-011-0636-6/TABLES/1>.
- [55] Z. Hasan, J. Jeon, S.H. Jung, Adsorptive removal of naproxen and clofibric acid from water using metal-organic frameworks, *J. Hazard. Mater.* 209–210 (2012) 151–157. <https://doi.org/10.1016/J.JHAZMAT.2012.01.005>.
- [56] F.X. Qin, S.Y. Jia, Y. Liu, H.Y. Li, S.H. Wu, Adsorptive removal of bisphenol A from aqueous solution using metal-organic frameworks, *New Pub Balaban.* 54 (2014) 93–102. <https://doi.org/10.1080/19443994.2014.883331>.
- [57] D. Roy, S. Neogi, S. De, Mechanistic investigation of photocatalytic degradation of Bisphenol-A using MIL-88A(Fe)/MoS₂ Z-scheme heterojunction composite assisted peroxymonosulfate activation, *Chem. Eng. J.* 428 (2022) 131028. <https://doi.org/10.1016/J.CEJ.2021.131028>.
- [58] H. Hu, H. Zhang, Y. Chen, Y. Chen, L. Zhuang, H. Ou, Enhanced photocatalysis degradation of organophosphorus flame retardant using MIL-101(Fe)/persulfate: Effect of irradiation wavelength and real water matrixes, *Chem. Eng. J.* 368 (2019) 273–284. <https://doi.org/10.1016/J.CEJ.2019.02.190>.
- [59] S. Ding, J. Wan, Y. Ma, Y. Wang, M. Pu, X. Li, J. Sun, Water stable SiO₂-coated Fe-MOF-74 for aqueous dimethyl phthalate degradation in PS activated medium, *J. Hazard. Mater.* 411 (2021) 125194. <https://doi.org/10.1016/J.JHAZMAT.2021.125194>.
- [60] H. Li, J. Wan, Y. Ma, Y. Wang, X. Chen, Z. Guan, Degradation of refractory dibutyl phthalate by peroxymonosulfate activated with novel catalysts cobalt metal-organic frameworks: Mechanism, performance, and stability, *J. Hazard. Mater.* 318 (2016) 154–163. <https://doi.org/10.1016/J.JHAZMAT.2016.06.058>.

- [61] J. Wang, J. Wan, Y. Ma, Y. Wang, M. Pu, Z. Guan, Metal–organic frameworks MIL-88A with suitable synthesis conditions and optimal dosage for effective catalytic degradation of Orange G through persulfate activation, *RSC Adv.* 6 (2016) 112502–112511. <https://doi.org/10.1039/C6RA24429G>.
- [62] E. Arany, R.K. Szabó, L. Apáti, T. Alapi, I. Ilisz, P. Mazellier, A. Dombi, K. Gajda-Schranz, Degradation of naproxen by UV, VUV photolysis and their combination, *J. Hazard. Mater.* 262 (2013) 151–157. <https://doi.org/10.1016/j.jhazmat.2013.08.003>.
- [63] H.F.D. Almeida, I.M. Marrucho, M.G. Freire, Removal of Nonsteroidal Anti-Inflammatory Drugs from Aqueous Environments with Reusable Ionic-Liquid-Based Systems, *ACS Sustain. Chem. Eng.* 5 (2017) 2428–2436. <https://doi.org/10.1021/acssuschemeng.6b02771>.
- [64] A. Ghauch, A.M. Tuqan, N. Kibbi, Naproxen abatement by thermally activated persulfate in aqueous systems, 279 (2020) 861–873. <https://doi.org/10.1016/j.cej.2015.05.067>.
- [65] H. Li, J. Wan, Y. Ma, Y. Wang, X. Chen, Z. Guan, Degradation of refractory dibutyl phthalate by peroxymonosulfate activated with novel catalysts cobalt metal-organic frameworks: Mechanism, performance, and stability, *J. Hazard. Mater.* 318 (2016) 154–163. <https://doi.org/10.1016/j.jhazmat.2016.06.058>.
- [66] T. Chalati, P. Horcajada, R. Gref, P. Couvreur, C. Serre, Optimisation of the synthesis of MOF nanoparticles made of flexible porous iron fumarate MIL-88A, *J. Mater. Chem.* 21 (2011) 2220–2227. <https://doi.org/10.1039/c0jm03563g>.
- [67] A. Baalbaki, N. Zein Eddine, S. Jaber, M. Amasha, A. Ghauch, Rapid quantification of persulfate in aqueous systems using a modified HPLC unit, *Talanta.* 178 (2018) 237–245. <https://doi.org/10.1016/J.TALANTA.2017.09.036>.
- [68] R. El Asmar, A. Baalbaki, Z. Abou Khalil, S. Naim, A. Bejjani, A. Ghauch, Iron-based metal organic framework MIL-88-A for the degradation of naproxen in water through persulfate activation, *Chem. Eng. J.* 405 (2021) 126701.
- [69] E.Y. Ionashiro, F.J. Caires, A.B. Siqueira, L.S. Lima, C.T. Carvalho, Thermal behaviour of fumaric acid, sodium fumarate and its compounds with light trivalent lanthanides in air atmosphere, *J. Therm. Anal. Calorim.* 108 (2011) 1183–1188. <https://doi.org/10.1007/S10973-011-1660-0>.
- [70] TRANSFER OF SELECTED PHARMACEUTICALS VIA WATER VAPOR UNDER MODERATE TEMPERATURES IN SOLAR STILLs, (n.d.). <https://scholarworks.aub.edu.lb/bitstream/handle/10938/10958/et-6444.pdf?sequence=1>.
- [71] Y. He, I. Hua, Photochemical reactions of ibuprofen, naproxen, and tylosin, *Abstr.*

- Pap. Am. Chem. Soc. 246 (2013).
- [72] J.L. Packer, J.J. Werner, D.E. Latch, K. McNeill, W.A. Arnold, Photochemical fate of pharmaceuticals in the environment: Naproxen, diclofenac, clofibrac acid, and ibuprofen, *Aquat. Sci.* 65 (2003) 342–351. <https://doi.org/10.1007/s00027-003-0671-8>.
- [73] V.M. Vulava, W.C. Cory, V.L. Murphey, C.Z. Ulmer, Sorption, photodegradation, and chemical transformation of naproxen and ibuprofen in soils and water, *Sci. Total Environ.* 565 (2016) 1063–1070. <https://doi.org/10.1016/j.scitotenv.2016.05.132>.
- [74] D.T. Oyekunle, J. Cai, E.A. Gendy, Z. Chen, Impact of chloride ions on activated persulfates based advanced oxidation process (AOPs): A mini review, *Chemosphere.* 280 (2021) 130949. <https://doi.org/10.1016/j.chemosphere.2021.130949>.
- [75] L. Zhao, Y. Ji, D. Kong, J. Lu, Q. Zhou, X. Yin, Simultaneous removal of bisphenol A and phosphate in zero-valent iron activated persulfate oxidation process, *Chem. Eng. J.* 303 (2016) 458–466. <https://doi.org/10.1016/J.CEJ.2016.06.016>.
- [76] X. Duan, C. Su, J. Miao, Y. Zhong, Z. Shao, S. Wang, H. Sun, Insights into perovskite-catalyzed peroxymonosulfate activation: Maneuverable cobalt sites for promoted evolution of sulfate radicals, *Appl. Catal. B Environ.* 220 (2018) 626–634. <https://doi.org/10.1016/J.APCATB.2017.08.088>.
- [77] Y. Liu, X. Chen, Y. Yang, Y. Feng, D. Wu, S. Mao, Activation of persulfate with metal–organic framework-derived nitrogen-doped porous Co@C nanoboxes for highly efficient p-Chloroaniline removal, *Chem. Eng. J.* 358 (2019) 408–418. <https://doi.org/10.1016/J.CEJ.2018.10.012>.
- [78] Z. Wei, F.A. Villamena, L.K. Weavers, Kinetics and Mechanism of Ultrasonic Activation of Persulfate: An in Situ EPR Spin Trapping Study, *Environ. Sci. Technol.* 51 (2017) 3410–3417. https://doi.org/10.1021/ACS.EST.6B05392/SUPPL_FILE/ES6B05392_SI_001.PDF.
- [79] T. Chalati, P. Horcajada, R. Gref, P. Couvreur, C. Serre, Optimisation of the synthesis of MOF nanoparticles made of flexible porous iron fumarate MIL-88A, *J. Mater. Chem.* 21 (2011) 2220–2227. <https://doi.org/10.1039/C0JM03563G>.
- [80] K.-Y.A. Lin, H.-A. Chang, C.-J. Hsu, Iron-based metal organic framework, MIL-88A, as a heterogeneous persulfate catalyst for decolorization of Rhodamine B in water, *Rsc Adv.* 5 (2015) 32520–32530.
- [81] M.J. Davies, B.C. Gilbert, J.K. Stell, A.C. Whitwood, Nucleophilic substitution reactions of spin adducts. Implications for the correct identification of reaction intermediates by EPR/spin trapping, *J. Chem. Soc. Perkin Trans. 2.* 0 (1992) 333–335. <https://doi.org/10.1039/P29920000333>.

- [82] H. Liu, T.A. Bruton, F.M. Doyle, D.L. Sedlak, In situ chemical oxidation of contaminated groundwater by persulfate: Decomposition by Fe(III)- and Mn(IV)-containing oxides and aquifer materials, *Environ. Sci. Technol.* (2014). <https://doi.org/10.1021/es502056d>.